

VOLUME 4
CHAPTER 21
Properties of CVI-SiC Matrix Composites

EDGAR LARA-CURZIO
Oak Ridge National Laboratory
Oak Ridge, TN 37831-6069 USA

December, 1999

Abstract

The mechanical and physical properties of fiber-reinforced chemical vapor infiltrated SiC-matrix composites are reviewed. Emphasis is given to the properties of composites reinforced with continuous fibers and 2-D fiber architectures, although the cases of composites reinforced with discontinuous fibers and other fiber architectures (e.g., 2.5D, 3-D) are also addressed. Experimental results are presented for elastic constants, tensile and shear strength in various material planes, interfacial properties, fracture resistance, performance-related behavior (e.g., thermal and mechanical fatigue, creep, stress-rupture, thermal shock resistance) and thermal and physical properties (e.g., thermal conductivity and diffusivity, thermal expansion, density). Environmental effects (e.g., oxidation, corrosion, neutron-irradiation) on mechanical performance and physical properties are also reviewed.

When appropriate, experimental results are discussed with respect to the role of the constituents and existing models. Experimental techniques and standardized test methods are briefly described.

CONTENTS

4.21.1	INTRODUCTION
4.21.1.1	Standardized Test Methods
4.21.2	MECHANICAL PROPERTIES
4.21.2.1	Elastic Properties
4.21.2.2	Monotonic Tensile Behavior
	In-Plane Tensile Behavior
	Trans-Thickness Tensile Behavior
4.21.2.3	Shear Properties
4.21.2.4	Interfacial Properties
4.21.2.5	Fracture Resistance
4.21.2.6	Residual Stresses
4.21.3	PHYSICAL PROPERTIES
4.21.3.1	Transport Properties
4.21.3.2	Thermal expansion
4.21.3.3	Thermal shock resistance
4.21.4	DURABILITY AND RELIABILITY
4.21.4.1	Matrix cracking
4.21.4.2	Mechanical Cyclic Fatigue
4.21.4.3	Creep and Stress-Rupture
4.21.5	ENVIRONMENTAL AND RADIATION EFFECTS ON PHYSICAL AND MECHANICAL PROPERTIES
4.21.5.1	Oxidation and Corrosion
4.21.5.2	Neutron Irradiation
4.21.6	COMPONENTS AND SPECIAL CONFIGURATIONS
4.21.7	SUMMARY

4.21.1 INTRODUCTION

As with all composite materials, the thermomechanical behavior and physical properties of chemically-vapor infiltrated (CVI) SiC matrix composites are determined by the properties of their constituents (i.e., fiber, fiber coating, matrix, matrix coating and their interfaces), by the architecture of the reinforcement, and by a number of micromechanical mechanisms that include matrix cracking and bridging of those cracks through fiber debonding and sliding. The synthesis and properties of ceramic fibers that have been used to reinforce CVI-SiC matrices were reviewed in Volume 1, while Chapter 26 in Volume 4 lists the various ceramic matrix composite systems currently available including CVI-SiC matrix composites. In Chapter 15 of Volume 4 the role of the fiber/matrix interface on the mechanics of deformation of continuous fiber-reinforced ceramic matrix composites (CFCCs) was reviewed in detail.

CVI is an extension of chemical vapor deposition (CVD) which is used for the synthesis of coatings. The basis of these two process are the same, but considerations of surface area and gas diffusion through channels formed by the reinforcement preform are important considerations for the former. Although several matrices have been successfully synthesized by CVI for the fabrication of ceramic matrix composites (Lackey and Starr, 1990; Lowden et al., 1995) CVI-SiC matrix composites have been by far the most widely used. SiC possesses many desirable properties for structural and non-structural applications at elevated temperatures such as: oxidation-resistance, low density, dimensional stability (low coefficient of thermal expansion and creep resistance), wear resistance, adequate thermal conductivity for thermal management, large stiffness, low activation under neutron irradiation, and although it has low fracture toughness, this can be readily improved by the incorporation of reinforcing fibers as

shown later in this chapter. In fact, one of the most important attributes of CFCCs, including CVI-SiC matrix composites, is their ability to retain their tensile strength in the presence of holes and notches. In CFCCs, elastic stress concentrations at holes and notches are alleviated by redistribution of stresses through various inelastic deformation mechanisms. This characteristic is important because components fabricated with CFCCs generally will need to be attached to other components and at these attachments (whether mechanical or bonded), stress concentrations will arise and dominate the design and reliability of the component (Evans et al., 1995).

Ceramic fiber preforms for CVI-ceramic matrix composites are routinely constructed utilizing two-dimensional fabric lay-ups. The need to maintain a reinforcement skeleton during matrix infiltration precludes the use of particulates or whiskers for reinforcing CVI-matrices, but short chopped fibers that can form mats can be used for this purpose and yield a product with reduced anisotropy¹ (Lowden et al., 1995). Because most of the CVI-SiC matrix composites currently available (and hence most characterized) are reinforced with 2-D continuous fiber architectures, the bulk of the data contained in this chapter corresponds to the properties of these materials. The most widely used fiber architecture is woven fabric (plain and satin weaves) but CVI-SiC matrix composites have also been densified with simpler (e.g., stacking unidirectional layers) or more complex (e.g., 2.5D and 3-D) fiber architectures.

Although most of the data available for fiber-reinforced CVI-SiC matrix composites is for composites reinforced with SiC-based fibers, CVI-SiC matrix composites have also

¹ Vacuum molding does not produce preforms with truly random orientation of the fibers, but instead the fibers tend to lie randomly in one plane and thus these preforms are generally more two-dimensional (Lowden et al., 1995).

been reinforced with carbon (Fitzer, 1988; Lacombe and Rouges, 1990; Lacombe and Bonnet, 1990) and oxide fibers [Lowden, 1988 #138] [Weaver, 1993 #13].

Carbon has been, by far, the most widely used fiber coating for CVI-SiC matrix composites. The primary roles of the fiber coating in these composites are: to protect the fibers during matrix synthesis and, to allow fiber debonding and fiber sliding in the wake of advancing cracks in the matrix. However, the lack of oxidation resistance of carbon in air at temperatures higher than 300°C has prompted extensive work in the development of oxidation-resistant fiber coatings for CVI-SiC matrix composites that include boron nitride (Rice, 1987; Naslain et al., 1991), doping carbon and BN with various elements (e.g. boron and silicon, respectively) (Lowden et al., 1993; Moore et al., 1995; Jacques et al., 1997), the use of multilayered fiber coatings (e.g. sequences of carbon and SiC) (Carpenter and Buhlen, 1992; Droillard, 1993; Naslain, 1995), low-strength porous and pseudo-porous fiber coatings (Carpenter and Buhlen, 1992; Carpenter et al., 1993; Hay, 1995; Ogbuji, 1995) and multilayered oxide coatings (Lee et al., 1998).

Additionally, various approaches have been followed to protect the interior of CVI-SiC matrix composites from oxidation and environmental attack. These include the addition of glass-formers in the matrix (Weddell and Ahluwalia, 1994; Fox and Nguyen, 1995; Lamouroux et al., 1999) and the use of environmental barrier coatings (Lee et al., 1994).

There have been limited studies comparing the properties and behavior of CVI-SiC matrix composites with those of other composites reinforced with the same fibers, fiber architecture, fiber volume fraction and fiber coatings, but different matrix. In one of those studies Sudre et al. compared the tensile properties and behavior of CVI-SiC and polymer-derived SiC matrix composites containing the same fiber preforms and fiber

coating (Sudre et al., 1995). The material used in that investigation consisted of a 6 mm-thick carbon fiber preform with a 0/90/ \pm 45 architecture using woven carbon fiber fabric stitched in the through-thickness direction. The fibers were coated with a layer of pyrocarbon of unspecified thickness. The polymer-derived SiC matrix, which required up to four infiltration cycles for densification, was denser than the CVI-SiC matrix, and unlike the CVI-matrix which had pores, the polymer-derived SiC matrix had crack-like defects. Under tensile loading, both materials exhibited non-linear behavior without an apparent proportional limit stress and the initial modulus of the CVI-SiC matrix composite was twice as large as that of the composite with the polymer-derived SiC matrix, although the former had larger residual strains and narrower loops upon cyclic loading/unloading/reloading to increasingly larger stress levels². Under tensile/tensile mechanical cyclic fatigue both composites exhibited similar behavior and were found to be fatigue insensitive for peak stresses up to 90 MPa. However, under cyclic tensile/compressive mechanical loading the composite with the polymer-derived SiC matrix failed after a few cycles when the peak stress was \pm 140 MPa. It is believed that the lower elastic modulus of the polymer-derived SiC may be responsible for allowing fiber buckling and hence for lower composite compressive strength.

4.21.1.1 Standardized Test Methods

Because the commercial diffusion and industrial acceptance of continuous fiber-reinforced ceramic matrix composites would be hampered by lack of standardized test methods, data bases or design codes, initial standardization efforts concurrent with the development of these materials in the United States have focused on methods for the

² For a discussion of residual stresses refer to section * of this chapter and chapter * of volume *.

mechanical evaluation of test specimens, and on the drafting of design codes (Lara-Curzio and Jenkins, 1999, Jenkins, 1999 #87) .

In the United States, the American Society for Testing and Materials (ASTM) has spearheaded the widespread introduction of standard test methods for advanced ceramics and ceramic composites. Since its establishment in 1991, ASTM subcommittee C28.07 on ceramic matrix composites has been responsible for formalizing nine full consensus standard test methods for CFCCs and for drafting several other documents that are currently undergoing ASTM's internal balloting process. In Europe, technical committee 184 of the Committee for European Normalization (CEN TC-184) is the organization responsible for the development of full-consensus test standards for CFCCs. To date, this organization has produced 14 provisional standards for CFCCs -which are listed in Table 1- some of which are in the process of becoming permanent standards. In Japan, the Petroleum Energy Center has been one of the organizations responsible for sponsoring the drafting, to date, of nine industry-accepted test standards for CFCCs. Recently, international harmonization activities have resulted in the drafting of four international standards for CFCCs (tension, compression, in-plane and interlaminar shear) within the jurisdiction of technical committee 206 on Advanced Technical Ceramics of the International Standards Organization (ISO TC-206), and it is expected that these activities will continue in the future. When appropriate, the availability of standard test methods for the determination of a particular CFCC property will be indicated in this chapter.

However, work is still needed towards the standardization of nomenclature and data reporting practices for ceramic matrix composites. For example, general references to

SiC/SiC composites are meaningless considering the many forms and types of SiC-based fibers, fiber coatings, fiber architectures, and forms of SiC matrices that are currently available. Lack of standardization in data reporting was most evident during the preparation of this document which in many cases hindered direct comparisons between materials and their properties.

Although the bulk of the mechanical data reported in the open literature for continuous fiber-reinforced CVI-SiC matrix composites has resulted from flexural (bending) tests, these results will not be reviewed here. The major disadvantage of flexural tests data for CFCCs is that despite the simplicity in the conduction of these tests, the determination of stresses from the experimentally-measured mechanical loads is not straightforward for stresses larger than the proportional limit stress. The equations that traditionally have been used to calculate “flexural strength” of continuous fiber-reinforced ceramic matrix composites, as a function of the applied mechanical load, are not applicable for these materials because continuous fiber-reinforced ceramic matrix composites are not homogeneous, and for stresses larger than the proportional limit stress, they are not perfectly elastic and do not exhibit symmetric behavior between tension and compression (Steif and Trojnacki, 1994; Raghuraman et al., 1996). In the absence of analyses to determine the actual stress distribution in a CFCC specimen subjected to bending as a function of the applied mechanical load, flexural experimental data will only be of value for comparing the response of specimens that possess identical dimensions, span, loading configuration, etc., which unfortunately are not the conditions for most of the results found in the literature.

4.21.2 MECHANICAL PROPERTIES

4.21.2.1 Elastic Properties

Various techniques have been used to determine the elastic properties of continuous fiber-reinforced CVI-SiC matrix composites. These include the recording of stresses and strains during mechanical loading within the elastic range, and the use of acoustic and small-amplitude vibration methods. Ultrasonic techniques have the advantage of being non-destructive and by aligning a particular direction of the material with the direction of propagation of the ultrasonic pulse, the elastic property of the material in that direction can be obtained. For example, the coefficients of the stiffness tensor of a material can be obtained by solving the following equation

$$\det (C_{ijkl} n_k n_l - \rho v^2 \delta_{ij}) = 0 \quad (1)$$

where C_{ijkl} are the coefficients of the stiffness tensor, n_i is the direction of propagation of the ultrasonic pulse, ρ is the density of the material, v is the phase velocity and δ is Kronecker's delta (El Bouazzaoui et al., 1996; Bouchetou et al., 1995).

Following this approach, Baste and co-workers determined the nine coefficients of the stiffness tensor for 2-D continuous fiber-reinforced CVI-SiC matrix composites (El Bouazzaoui et al., 1996). Experimentally, they obtained wave velocity measurements of ultrasonic pulses refracted through the sample while the sample was immersed in a water tank. At each stress level the phase velocities of quasi-longitudinal and quasi-shear bulk waves exiting the sample were measured as a function of the transmission angle and a special signal processing method was necessary to account for the signal distortion that occurs as a result of the porous internal structure of the material. These measurements

yielded a modulus in one of the fiber directions of carbon fiber-reinforced CVI-SiC of 118 ± 4 GPa (2-D, plain weave, PAN-precursor carbon fibers (3000 fibers/bundle) coated with a 1 μm -thick layer of pyrocarbon, fiber volume fraction of 40%, 10-15 % residual porosity and composite density of 2.0 g/cc) which compares well with that obtained by mechanical means $115 \text{ GPa} \pm 12$ for the same material (Camus et al., 1996).

Hsu and co-workers found through this type of measurements that the stiffness of 2-D CG-Nicalon™ fiber reinforced CVI-SiC CFCCs decrease linearly with the volume fraction of porosity in accordance with Equation (1) (Hsu et al., 1995).

Another approach for the determination of Young's and the shear moduli consists in determining the natural frequencies of the flexural and torsional modes of vibration of a rectangular beam using a fast Fourier transform spectrum analyzer and beam theory. For example, Sakata et al. determined the elastic properties of CG-Nicalon™/CVI-SiC in ambient air between room temperature and 1200°C (Sakata and Ohnabe, 1997). The material studied had a density of 2.58 g/cm³ and consisted of carbon-coated plain weave fabric of CG-Nicalon™ fibers that occupied a volume fraction of 40%. There was 9.7% porosity in the matrix which contained an enhancement of proprietary composition³. The orthotropic elastic constants were computed from the measured natural frequencies of specimens of dimensions 3 mm x 4 mm x 50 mm that had been obtained from a square plate. Table 2 lists the results.

Measurements at elevated temperatures showed that the elastic constants of this material decreased with temperature for temperatures above 600°C, but that the magnitude of the

³ “Enhanced SiC”. Allied Signal Composites. Newark, DE 19714

elastic constants increased with time thereafter while the specimen was held at the test temperature. The initial loss of stiffness was associated with the oxidation of the carbonaceous fiber coating whereas the subsequent increase was associated with the formation of SiO_2 at the fiber matrix interface as a result of fiber and matrix oxidation. Additional discussion of environmental effects on mechanical properties can be found in section * of this chapter.

The effect of fiber architecture on the elastic constants of CG-NicalonTM/CVI-SiC matrix composites was investigated by Stiff (Stiff, 1993). The material evaluated had a density of 2.54 g/cm^3 and consisted of eight plies of carbon-coated (unspecified fiber coating thickness) 8-harness satin weave fabric of CG-NicalonTM. The total fiber volume fraction was 33%. The elastic constants were determined from stress-strain measurements within the elastic regime using strain gauges adhesively bonded to straight-sided tensile specimens that had been processed with orientations of 0/90, 0/90 \pm 45, and \pm 45 with respect to the loading direction. The results, which are summarized in Table 3, indicate that Young's modulus along the loading direction decreases with increasing number of 45° layers, while the opposite trend was found for the in-plane shear modulus.

Chulya et al. determined the elastic modulus of CVI-SiC matrix composites reinforced with a 3-D architecture of CG-NicalonTM fibers at ambient temperature, 1200°C and 1550°C through tensile tests of dog-bone shaped specimens (Chulya et al., 1992). The specimens consisted of 5-harness satin weave fabric with an angle interlock between layers. The preform was woven as a flat panel with a fiber volume fraction of 41% and then coated with a 0.5-1.0 μm thick layer of pyrocarbon. The matrix had 10-15% porosity and the specimens were coated, after machining with a multilayered oxidation-

resistant coating. The elastic modulus was found to be 237 GPa at ambient temperature, 258 GPa at 1200°C and 60 GPa at 1550°C.

Typical values for Young's modulus, Poisson's ratio and shear modulus along the principal directions of fiber-reinforced CVI-SiC matrix composites are listed in Table 4.

4.21.2.2 Monotonic Tensile Behavior

In-Plane Tensile Behavior

Among the first standards developed for the mechanical evaluation of CFCCs were the standards for tensile strength at ambient and elevated temperatures (See Table 1). Recently, a round-robin testing program was completed in the U.S. to determine precision and bias statements for ASTM test standard C1275 "Standard Test Method for Monotonic Tensile Strength Testing of Continuous Fiber-Reinforced Advanced Ceramics with Solid Rectangular Cross-Section Specimens at Ambient Temperatures" (ASTM, 1995). From this study coefficients of variation for repeatability and reproducibility were obtained for elastic modulus, proportional limit stress, ultimate tensile strength and strain at fracture of a "model material". However, no statement of bias was given because no acceptable reference standard material exists.

Previously, a study had been conducted to verify the usability of this test method by evaluating the effects of specimen geometry, mechanical loading rate, and loading mode (force versus displacement control) on the tensile strength and stress-strain behavior of a CVI-SiC matrix composite (Piccola et al., 1997). The material used in that investigation consisted of twelve plies of plain-weave fabric of CG-Nicalon™ fibers coated with a 0.3 μm-thick layer of carbon. The fibers occupied 40% of the volume of the composite and

the matrix had 15-20% residual porosity. Tests were conducted at ambient air and temperature. It was found that neither the test mode (displacement vs. mechanical load control) or test rate (50 N/S vs. 500 N/s; 0.003 mm/s vs. 0.03 mm/s) had an effect on the proportional limit stress or ultimate tensile strength of the material. Although the geometry of the test specimens did not have an effect on the proportional limit stress, it was found that contoured tensile specimens with the smallest gauge length had the largest tensile strength. Also, although the amount of percent bending did not affect the ultimate tensile strength of the material (probably because the ultimate tensile strength is controlled by fiber ligaments of large aspect ratio that bridge the critical matrix crack), it did have an effect on the proportional limit stress which decreased with increasing percent bending. Currently, a maximum percent bending strain of 5% is prescribed by both ASTM C1275 and the ISO test standard on tensile strength that will become available soon.

Figure 1 shows a typical tensile stress-strain curve for a unidirectional Hi-Nicalon™-reinforced CVI-SiC with a thin fiber coating of pyrocarbon and a fiber volume fraction of 40%. This curve exhibits well-defined regimes associated with: (a-b) linear elastic behavior up the proportional limit stress (b-c) and elastic/non-linear inelastic behavior for larger stresses. The three mechanisms responsible for the non-linearity exhibited in the tensile stress-strain curves of most continuous fiber-reinforced ceramic matrix composites are (Evans et al., 1995): (1) Matrix cracking; (2) Changes in the residual stress distribution as a result of matrix cracking. The relative ability of these mechanisms to operate will depend on the loading conditions, as well as the fiber orientation; (3) frictional dissipation that occurs at the fiber/matrix interfaces and that is dominated by the fiber coating, the fiber morphology and the topography of the fiber's surface. By

varying the magnitude of the interfacial shear stress, the prevalent damage mechanism and the resultant non-linear stress-strain behavior can be dramatically modified.

Analyses of damage and failure of CFCCs have established that certain constituent properties are basic to composite performance. These independent parameters include: the interfacial sliding stress, the fiber debond energy, the in-situ fiber characteristic strength and Weibull modulus, the fiber/matrix misfit strain, and the matrix fracture energy (Evans et al., 1995). Dependent parameters that can often be used to infer the constituent properties include: the fiber pull-out length, the fracture mirror radius on the fibers and the saturation crack spacing in the matrix.

In most composites with desirable tensile properties, linear elastic fracture mechanics criteria are violated. In consequence, alternate mechanics are needed to specify the material and loading parameters that are relevant to establish design rules for their manufacture and the fabrication of components. For CFCCs, this has been achieved using large-scale bridging mechanics combined with continuum damage mechanics (Evans et al., 1995, Gasser, 1996 #73).

Figures 2 and 3 summarize the tensile strength results for several continuous fiber-reinforced CVI-SiC matrix composites at different temperatures. Included in these graphs are data for composites reinforced with CG-Nicalon™ fibers, Hi-Nicalon™ fibers, T-300 graphite fibers, PAN-derived graphite fibers, Sumitomo® alumina fibers, and various grades of Nextel™ fibers. For composites with comparable fiber concentration and architecture, CVI-SiC matrix composites reinforced with graphite fibers exhibit the highest tensile strength, and in inert environment, the best retention of

strength at elevated temperatures. Figure 4 illustrates the effect of fiber type on the tensile stress-strain curve of CVI-SiC matrix composites. One curve corresponds to a composite reinforced with CG-Nicalon™ fibers while the other corresponds to a composite reinforced with Hi-Nicalon™ fibers. Both materials consisted of 5 harness satin weave fabric, coated with a thin layer of pyrocarbon, and the CVI-SiC matrix contained an oxidation-resistance enhancement of proprietary composition³. The effect of fiber stiffness (200 GPa for CG-Nicalon™ versus 350 GPa for Hi-Nicalon™) on the stiffness of the composite and on the magnitude of the proportional limit stress is evident in Figure 3. Figure 5 shows a collection of stress-strain curves of Hi-Nicalon™ fibers in a CVI-SiC matrix with multilayered fiber coatings of carbon and SiC to illustrate the reproducibility and variability in strength of this material in air at 950°C.

Figure 6 shows the stress-strain curves of oxide (Sumitomo® 85% γ -alumina and 15% SiO₂) and carbon (Bestfight™) fiber-reinforced CVI-SiC. In both cases the fiber architecture consisted of plain weave fabric coated with a layer of carbon 0.5 to 1 μ m in thickness. In both materials the volume fraction occupied by the fibers was 40% and the residual porosity in the matrix was 20%. Tensile tests were conducted both at room temperature and 1100°C and was found that both materials exhibited elastic behavior up to 100 MPa and had a tensile strength between 160 and 200 MPa and strain at failure between 0.4 and 0.5 % (Steen and Vallés, 1997). The major differences in the behavior of these materials, as reflected by the shape of the tensile stress-strain curves can be explained based on the difference in the state of residual stresses of the fibers and matrix (See Section *).

Camus and Barbier (Camus and Barbier, 1995) studied the mechanical response of 2-D carbon fiber-reinforced CVI-SiC under loading/reloading conditions between room temperature and 1600°C. The PAN-precursor carbon fibers occupied 40% of the composite volume and the matrix had residual porosity between 10-15%. Tests were conducted at a rate of 20 MPa/second using 125 mm-long specimens for the tests at room temperature and 190 mm-long specimens for the tests at elevated temperatures. The elevated temperature tests were conducted in argon. As a result of residual strains, extensive matrix cracking and fiber debonding were evident in the as-processed state, and under tensile loading no linear regime was observed in the stress-strain curves and the behavior was found to be non-linear up to failure. Figure 2 shows a summary of the tensile results whereas Figure 7 shows the evolution of the residual strains observed upon unloading as a function of the applied stress for various temperatures.

Effinger et al. (Effinger et al., 1996) reported tensile data for continuous fiber-reinforced CVI-SiC up to 1650°C. The materials evaluated in this investigation consisted of a 2-D plain weave fabric (0/90) of either T300® fibers (1000 fibers/tow) or CG-Nicalon™ fibers (500 fibers/tow). Both materials had a fiber volume fraction of 40% and tests were conducted with dog bone-shaped tensile specimens at a loading rate of 400 MPa/min for CVI-SiC matrix composites reinforced with CG-Nicalon™ fibers and 200 MPa/min for CVI-SiC matrix composites reinforced with carbon fibers. The tensile strength of composites reinforced with carbon fibers was 530 MPa up to 815°C in air which was maintained up to 1650°C. CG-Nicalon™/SiC exhibited a maximum strength of 285 MPa at 980°C which decreased to 180 MPa at 1480°C. Figures 2 and 3 show a summary of the tensile results for carbon fiber and Nicalon™ fiber-reinforced composites.

The effect of fiber architecture on the tensile strength of CG-Nicalon™-reinforced CVI-SiC matrix composites was investigated by Stiff (Stiff, 1993). The material evaluated had a density of 2.54 g/cm^3 and consisted of eight plies of carbon-coated (unspecified fiber coating thickness) 8-harness satin weave fabric of CG-Nicalon™, occupying 33% of the composite volume. The laminates were processed with orientations of 0/90, 0/90 \pm 45, and \pm 45 with respect to the loading direction and tests were conducted with straight-sided specimens. The results are summarized in Table 5 and show mild dependence of the proportional limit stress with fiber architecture although strength was largest for the specimens evaluated in the 0/90 configuration and smallest in the \pm 45° configuration.

Chulya et al. determined the tensile strength of CVI-SiC matrix composites reinforced with a CG-Nicalon™ fiber 3-D architecture at ambient temperature, 1200°C and 1550°C (Chulya et al., 1992). The fiber architecture consisted of 5-harness satin weave (0/90) and an angle interlock between each layer. The fibers occupied 41% of the volume and were coated with pyrolytic carbon layer 0.5-1.0 μm thick. The matrix porosity was about 10 to 15 % and the composite was coated for oxidation protection. The ultimate strength of this material was 139 MPa at ambient temperature, 122 MPa at 1200°C and 66 MPa at 1550 °C while the failure strain increased from 0.22% at ambient temperature and 1200°C to 0.57% at 1550°C.

Transthickness Tensile Behavior

Because of the availability of ceramic fibers in tows and fabric form, most fiber preforms for CVI-SiC matrix composites consist of stacked layers of woven fabric. As a

consequence of the resulting laminated structure, the composite exhibits large anisotropy between its in-plane and through-the-thickness physical and mechanical properties.

Depending on the characteristics of the composite system, the interlaminar shear, and transthickness tensile modes of failure of 1-D and 2-D continuous fiber-reinforced CVI-SiC matrix composites will be dominated either by the properties of the matrix or by those of the fiber/matrix interface.

This results in part, from the traditional emphasis in optimizing the mechanical properties of continuous fiber-reinforced ceramic matrix composites (maximization of in-plane tensile strength and toughness) by engineering of the fiber/matrix interface. Interfacial engineering in CVI-SiC matrix composites usually implies tailoring the fiber/matrix interface to achieve “weak” fiber bonding. However, weak fiber bonding will invariably result in poor interlaminar shear and transthickness tensile properties. Figure 8 shows the stress-strain curves obtained from the transthickness tensile evaluation of unidirectional Hi-Nicalon™/CVI-SiC matrix composites with pyrocarbon fiber coating, in a direction normal to the fiber direction. The specimens were square in size (10 mm x 10 mm) and 2.3 mm thick. In this case, failure occurred along a plane that coincides with the fiber/matrix interface at a stress level lower than the matrix cracking stress. For this material, the ratio of the transthickness tensile strength to the tensile strength along the fiber direction was found to be 0.025, which illustrates the large degree of anisotropy in the strength of the material.

Percival et al. determined the transthickness tensile strength of 2-D CG-Nicalon™/CVI-SiC⁴ by using circular specimens 15 mm in diameter that were bonded to tabs (Percival et al., 1997). The specimens were thicker than normal (7 mm thick) and were instrumented with adhesively-bonded strain gauges to record strains during the test. The transthickness tensile strength was found to be 13 MPa, and the strain to failure 0.016%. The curves were linear up to failure and the elastic modulus was found to be 80 GPa.

4.21.2.3 Shear Properties

The matrix cracking that occurs in 2-D CFCCs when subjected to shear loading depends on the loading orientation and the properties of the matrix. Two dominant loading orientations are of interest: in-plane shear and interlaminar shear. For the case of interlaminar shear, matrix cracks evolve without significant interaction with the fibers. Conversely, for in-plane shear loading, matrix cracks must interact with the fibers which impede crack development. Consequently, the in-plane shear strength always exceeds the interlaminar shear strength (Evans et al., 1995).

Analysis of experimental shear strength data indicates that the matrix has a major influence on the shear strength and the shear ductility of continuous fiber-reinforced ceramic matrix composites (Evans et al., 1995). Among the various matrices available, CVI-SiC has one of the largest shear moduli and consequently CVI-SiC matrix composites exhibit some of the largest in-plane shear strengths among CFCCs. The shear flow strengths of various CFCCs can be ranked using a parameter given by

$$W = \sqrt{\frac{\Gamma_m}{r G}} \quad (2)$$

⁴ CERASEP 347. SEP, France

where Γ_m is the fracture energy of the matrix, G is the shear modulus of the matrix, and r is the fiber radius.

The shear ductility also appears to be influenced by the shear modulus, but in the opposite sense, i.e., high modulus matrices result in composites with low in-plane shear ductility.

Currently, shear strength standards for CFCCs exist in the U.S., Europe and Japan, and work is underway to draft international standards within the ISO for the determination of in-plane and interlaminar shear strength. (See Table 1). Most standardized tests methods for the determination of in-plane shear strength of CFCCs are based on the use of the Iosipescu test, whereas the most widely used test method for the determination of interlaminar shear strength is the compression of double-notched specimens. Figures 9 and 10 show schematics of these tests.

Lara-Curzio and Ferber determined the in-plane shear strength of CG-Nicalon™ /CVI-SiC using the Iosipescu test (Lara-Curzio and Ferber, 1997a). The material used in that investigation consisted of 12 layers of plain weave fabric coated with a 0.3 μm -thick layer of carbon. The fibers occupied 40% of the volume of the composite and the matrix had 15-20% residual porosity. The specimens were 76 mm long, 19 mm wide and the separation between notches was 11 mm. The results were very repeatable and the shear strength was found to be 101 ± 4.7 mm. Figure 11 shows a micrograph of the gauge section of a Iosipescu CG-Nicalon™/CVI-SiC specimen after the test.

Fang and Chou determined the interlaminar shear strength of T-300® carbon and CG-Nicalon™ fiber-reinforced CVI-SiC by the compression of double-notched specimens (Fang and Chou, 1993). The materials consisted of 2-D plain weave fabric with volume fractions and densities of 45% and 40% and 2.1 and 2.5 g/cm³, respectively. The dimensions of the specimens were: 20.3 mm in length and 10.15 mm in width, while the notch separation was 3.18 mm. The interlaminar shear strength for carbon fiber-reinforced CVI-SiC ranged between 19 and 35 MPa, whereas that for CG-Nicalon™ fiber-reinforced CVI-SiC varied between 32 and 77 MPa.

Lara-Curzio and Ferber found that both the notch separation and the thickness of the fiber coating influence the magnitude of the apparent interlaminar shear strength when determined by the compression of double-notched specimens (Lara-Curzio and Ferber, 1997a). Figure 12 summarize the experimental results for 2-D CG-Nicalon™/CVI-SiC composites and compare those results with those of other composite materials. The dependence of the apparent interlaminar shear strength with notch separation was found to result from the interaction of the stress fields that emanate from the notches. For short notch separations, the interaction of the stress fields tends to decrease the magnitude of the stress concentration at the root of the notches, resulting in larger failure loads and hence higher interlaminar shear strengths. As the notches move farther apart and the interaction between the stress fields decrease, higher failure loads are required to initiate shear failure. As a consequence, it is believed that friction between the specimen and the fixture, and the clamping stress that results from Poisson's expansion and bending (the latter associated with the non-symmetric nature of the specimen) tend to increase the clamping force that in turn, alleviating thus the magnitude of the stress concentration and results in higher failure loads. The dependence of the apparent interlaminar shear

strength with increasing thickness of the fiber coating can be rationalized considering that the weak links in 2-D CFCCs subjected to interlaminar shear loading are: the matrix and the fiber coating. When the thickness of the fiber coating is larger than a critical value, the fiber coating itself becomes the weakest link, whereas for fiber coating thicknesses less than the critical value, the porosity-rich matrix interlaminar region becomes the weakest link.

Stiff determined the effect of fiber architecture on the in-plane and interlaminar shear strength of CG-Nicalon™/CVI-SiC (Stiff, 1993). The material evaluated had a density of 2.54 g/cm³ and consisted of eight plies of carbon-coated (unspecified fiber coating thickness) 8-harness satin weave fabric of CG-Nicalon™, occupying 33% of the composite volume. Laminates with orientations of 0/90, 0/90±45, and ±45 were evaluated. Although the proportional limit shear stress did not change with fiber architecture, the in-plane shear strength increased with the number of 45° layers. The results are summarized in Table 6. Conversely, no effect of fiber architecture was found on the interlaminar shear strength of these materials which were conducted by compressing double-notched specimens (50 mm x 20 mm) with a notch separation of 5 mm using an anti-buckling fixture. The fact that there is no effect of fiber architecture on the interlaminar shear strength is consistent with the fact that this property is controlled by the fiber/matrix interface.

Effinger et al. (Effinger et al., 1996) determined the interlaminar shear strength of CVI-SiC matrix composites up to 1650°C. The tests were conducted by the compression of double-notched specimens that had a reduced-width gauge section (16 mm-wide). The notch separation was 12.7 mm. The materials used in the investigation consisted of a 2-D

plain weave fabric (0/90) of either T300®™ fibers (1000 fibers/tow) or CG-Nicalon™ fibers (500 fibers/tow). Both materials had a fiber volume fraction of 40%. Tests at elevated temperatures were conducted in helium at a loading rate of 70 MPa/min for composites reinforced with carbon fibers and 35 MPa/min. for composites reinforced with CG-Nicalon™ fibers. At 1650°C the average interlaminar shear strength of CG-Nicalon™/CVI-SiC was found to be 40 MPa while it was 66 MPa for T300™/CVI-SiC. The results are summarized in Figure 13.

Xu et al. (Xu et al., 1999) determined the interlaminar shear strength of carbon fiber-reinforced CVI-SiC matrix composites with 3-D fiber architectures by the 3-point bending of beams with short span. The specimen dimensions were 2.5 x 5 x 40 mm and values between 10.7 and 22 MPa were obtained. It was found that the properties of the composite increased with increasing density. As with most test methods used for the determination of interlaminar shear strength, the stress distribution in a beam of short span subjected to 3-point bending is not uniform and this test method typically produces the largest shear strength values amongst all the available test techniques for composites (Sawyer, 1988). Furthermore, this test has all the drawbacks of flexural testing for ceramic matrix composites that were outlined in the introduction.

4.21.2.4 Interfacial Properties

Many techniques have been developed for the determination of interfacial properties of continuous fiber-reinforced ceramic matrix composites. Among the properties that characterize the behavior of the fiber/matrix interface, fiber bond strength, coefficient of friction and the fiber clamping residual stress are the properties of most interest. The techniques developed for the determination of these properties include single-fiber push-

in and push-out tests, single fiber and bundle pull-out tests, bundle push-in tests (Lara-Curzio and Ferber, 1995) and the tensile evaluation of microcomposites (Lamon et al., 1995) and minicomposites (Morscher and Martinez-Fernandez, 1999).

Abbe and Chermant (Abbe and Chermant, 1990) determined the interfacial shear stress in CG-NicalonTM/CVI-SiC specimens that had been subjected to “creep” in three-point bending in vacuum at temperatures between 1000°C and 1200°C. The interfacial shear stress was estimated through single-fiber push-in tests that were conducted using a micro-hardness indenter and an analysis that neglected the Poisson's expansion of the fibers during indentation. It was reported that the interfacial shear stress decreased with creep-test temperature from 21 MPa for as-processed materials to 3 MPa after creep testing at 1200°C but no details about the nature or the thickness of the fiber coating were provided.

Sudre et al. (Sudre et al., 1993) determined the interfacial debond energy, interfacial shear stress and fiber residual stress using an instrumented microindentation apparatus by means of push-in testing. Samples were obtained from composites fabricated with 0/90 plain weave fabric and coated with a thin layer of pyrocarbon of unspecified thickness. The interfacial parameters (which were obtained through an analysis that neglects the fiber's Poisson's expansion) are listed in Table 7.

Lara-Curzio et al. (Lara-Curzio et al., 1994) investigated the effect of fiber coating thickness on the interfacial properties of CG-NicalonTM/CVI-SiC matrix composites. The materials studied consisted of plain weave fabric of CG-NicalonTM fibers stacked with each layer rotated 30° with respect to its neighbors. The thicknesses of the fiber coating

was varied between 0.03 μm and 1.25 μm and the resulting range of density and fiber volume fraction in the composites were 2.22-2.65 g/cc and 39.5-43.7 %, respectively. The effective interfacial shear stress of the material was found to decreased from 24.6 ± 9.9 MPa for a composites with a fiber coating thicknesses of 0.03 μm to 3.8 ± 1.4 MPa for a composite with a fiber coating thickness of 1.25 μm (Figure 14). It was concluded that the decrease in the interfacial shear stress with increasing fiber coating thickness resulted from the simultaneous decrease of the coefficient of friction and the clamping residual stress with increasing coating thickness. On one hand, as the thickness of the fiber coating increases, the interaction between the topographic features of the fiber surface and those of the matrix can be eliminated by the compliant nature of the carbonaceous fiber coating. On the other hand, the magnitude of the residual radial clamping stress in the fiber, and hence the interfacial shear stress, decreases with increasing fiber coating thickness.

Rebillat and Lara-Curzio (Lara-Curzio et al., 1995; Rebillat et al., 1998b; Rebillat et al., 1998a) studied the interfacial characteristics of a new family of CG-Nicalon™/CVI-SiC composites with “strong” fiber bonding. In these materials, the fibers had been subjected to a proprietary treatment that resulted in composites exhibiting higher in-plane tensile strength and toughness as compared with CVI-SiC matrix composites reinforced with conventional CG-Nicalon™ fibers (Droillard, 1993). Microstructural analyses of composites with treated fibers revealed that cracks propagating through the matrix had deflected and branched into the fiber coating. Figure 15.a shows a stress versus fiber-end displacement obtained from a single-fiber push-out test for a composite with as-received CG-Nicalon™ fibers, whereas Figure 15.b shows the curve obtained from a similar test for a composite with treated CG-Nicalon™ fibers. Note the difference in the shape of the

curves and the magnitude of the stresses which are associated with either debonding along a single plane for the case of conventional materials or debonding along multiple planes as a result of crack branching in composites with treated fibers. The insets in Figures 15.a and 15.b are scanning electron micrographs of pushed-out fibers for composites with treated and untreated fibers. The roughness of the sliding surface of the composite with treated fibers is evident, in sharp contrast to the rather smooth sliding surface of untreated fibers. In the case of the former, debonding occurred within the fiber coating, whereas in the case of the latter, debonding occurred along a single plane between the fiber and the carbonaceous fiber coating. The interfacial shear stress of composites with untreated CG-Nicalon™ fibers was found to be 11 ± 4 MPa, whereas that for composites with treated fibers was 200 ± 40 MPa.

Lamon et al. (Lamon et al., 1995) obtained estimates of the interfacial properties of CVI-SiC matrix composites by using analytical solutions for the problem of interface debonding and fiber sliding to analyze hysteresis loops when microcomposite test specimens (single-fiber test specimen) are subjected to repeated mechanical loading/unloading. Table 8 lists the values obtained for the interfacial shear stress and debond energy of carbon- and boron nitride-coated CG-Nicalon™ fibers in a CVI-SiC matrix.

Morscher and Martínez-Fernandez (Morscher and Martinez-Fernandez, 1999) determined the interfacial shear stress of BN-coated CG-Nicalon™, Hi-Nicalon™ and Sylramic® fiber-reinforced CVI-SiC minicomposites from the analysis of hysteresis loops and measurements of matrix crack spacing and the results are listed in Table 9.

4.21.2.5 Fracture Resistance

Failure mechanisms and processes in continuous fiber-reinforced ceramic matrix composites during stable fracture are not merely confined to a localized region at the crack tip but include crack bridging, crack deflection, multiple matrix cracking and fiber pull-out over a larger fracture process zone (Gomina et al., 1987; Stull and Parvizi-Majidi, 1991). Therefore, the nature of the fracture process in these materials precludes the application of linear elastic fracture mechanics (LEFM). In spite of this, many have made, and continue making use of the existing LEFM formalism for the analysis of fracture resistance of continuous fiber-reinforced CVI-SiC matrix composites. Others have modified existing LEFM formalisms by employing concepts such as the equivalent elastic crack concept. For example, using single edge-notched beams, Heraud and Patrick (Heraud and Spriet, 1988) reported fracture toughness values between 30 to 35 MPam^{0.5} for carbon fiber and CG-NicalonTM-reinforced CVI-SiC composites.

The fracture resistance of continuous fiber-reinforced CVI-SiC matrix composites has also been quantified by adopting an energy approach in which fracture is expressed via an R-curve. R-curves characterize a material's resistance to fracture during slow, stable crack propagation and are dependent on the nature of the process zone extending from the crack tip in the material. Stull and Parvizi-Majidi investigated the fracture resistance of 2D (plain weave fabric) CG-NicalonTM/CVI-SiC matrix composites using Chevron-notched bend specimens tested in an edgewise configuration in which the crack propagated perpendicular to the ply direction (Stull and Parvizi-Majidi, 1991). R-curves were obtained from repeated loading and unloading and the experimental results were analyzed using several methods of data reduction. Values corresponding to the plateau

regions of the R-curves were taken as steady state crack growth resistance, and following three different approaches, obtained energy values ranged between 2.6 and 2.8 kJ/m².

Yang et al. (Yang et al., 1991) determined the fracture toughness of CVI-SiC matrix composites with two types of CG-NicalonTM fiber preforms; a 3-D braided structure and a 2-D structure consisting of plain weave fabric with each layer rotated 30° with respect to its neighbors. Both materials were densified simultaneously and the braided panel had a density of 2.6 g/cm³, a fiber volume fraction of 32% and 11% residual porosity, whereas the 2-D laminate had a fiber volume fraction of 35%, 15% porosity and a density of 2.3 g/cm³. Fracture toughness values were obtained using single edge notched beams (5 mm x 5 mm x 25 mm with a lower span of 18.75 mm) tested in 3-pt bending at a cross-head speed of 0.5 mm/min and following standard test method ASTM E399 (ASTM, 1991). Tests were conducted at room temperature after the specimens had been heat-treated at 1200°C for 100 hrs. Table 10 list the results and demonstrate that composites with 3-D fiber architecture are tougher than those with 2-D architecture.

Nair and Wang (Nair and Wang, 1992) investigated the fracture resistance of 2-D CG-NicalonTM/CVI-SiC up to 1200°C using compact tension specimens. The material used in their study had 8 plies of plain weave fabric and there was about 10% porosity in the matrix, mostly in the form of large pores associated with spaces in the fabric weave that were not infiltrated. The specimens were 63.5 mm x 44.5 mm, and the notch was 28.6 mm long and had a 200 µm-long slot. Crack opening displacements were determined optically and for the experiments at 1200°C the crack length was measured by unloading and cooling the specimen to room temperature after each cycle. The fracture resistance was obtained from compliance measurements of initially un-bridged cracks of different

lengths using the linear elastic strain energy release parameter for R-curve evaluation. It was found that the fracture resistance of the material increased from $14 \text{ MPa m}^{0.5}$ to $27 \text{ MPa m}^{0.5}$ at ambient temperature, which was attributed to fiber bridging of the primary crack and microcracking zone in the wake of the crack. At 1200°C the R-curve behavior was reduced and almost no crack bridging was observed. Fracture resistance values obtained at 1200°C were in the range of $12\text{-}18 \text{ MPa m}^{0.5}$. Using a J-integral technique in the regime of primary crack extension, Nair and Wang (Nair and Wang, 1998) determined that raising J_R -curve behavior started at 1500 J/m^2 and reached a value 6150 J/m^2 after 13 mm of primary crack extension.

Stiff (Stiff, 1993) evaluated the fracture toughness of CG-Nicalon™/CVI-SiC using the conventional LEFM formalism. The material evaluated had a density of 2.54 g/cm^3 and consisted of eight plies of carbon-coated (unspecified fiber coating thickness) 8-harness satin weave fabric of CG-Nicalon™ occupying 33% of the composite volume. Laminates with orientations of 0/90, 0/90±45, and ±45 with respect to the loading direction were evaluated. Fracture toughness values were determined using 50 mm x 10 mm single-edge-notched beams in bending with a notch 2.55 mm long and 1.7 mm wide. No details about the data reduction were provided for the numerical values listed in Table 11 which were obtained for composites with different fiber architectures.

Mizuno and co-workers (Mizuno et al., 1994) determined the fracture toughness and fracture energy of 2-D CG-Nicalon™/CVI-SiC composites. The materials studied consisted of 11 layers of plain weave fabric oriented in either the (0/90) or ±45° configuration. The fiber volume fraction was 40% while the density of the composite was 2.58 g/cm^3 . Tests were conducted using single-edge notched specimens tested in

tension with values for the ratio of notch length to specimen width between 0.2 and 0.6. The effective fracture energy was calculated as the work of fracture divided by the un-notched area perpendicular to the loading direction and values between 2.5 and 3.0 kJ/m² were obtained, whereas fracture toughness values were found to be between 14 and 30 MPam^{0.5}.

Lamon et al. (Droillard et al., 1995) developed expressions to predict the contributions of the size of the process zone and the initial notch length to the strain energy release rate. It was shown that fracture size effects for 2-D CG-NicalonTM fiber-reinforced CVI-SiC matrix composites are satisfactorily described using such relationship (in contrast to the use of an elastically equivalent notch length), and that this relation is independent of specimen size and geometry. A value of 10 kJ/m² was obtained for the intrinsic fracture energy of the material. The expression that these authors obtained for the fracture energy highlights the relationship between significant increases in toughening and increases in compliance, which may be achieved through extensive matrix microcracking.

Droillard and Lamon (Droillard and Lamon, 1996) investigated the fracture resistance of 2-D (plain weave fabric) CG-NicalonTM/CVI-SiC matrix composites with multilayered fiber coatings of carbon and SiC. Experimental measurements were obtained using compact tension specimens 25 mm x 25 mm with thicknesses between 3 and 5 mm. In addition, materials were prepared with treated fibers following a proprietary process that results in improved adhesion between the fibers and the carbon coating (“strong bonding”) (Droillard, 1993). The fracture toughness was determined from both the value of the J-integral at maximum load when the macroscopic crack initiates at the notch tip within the process zone, and from the strain energy release rate. The results show that the

data can be grouped in sets of high and low values of strain energy release rate, depending on whether the fibers were treated or not. Toughness values ranged between 12 and 30 kJ/m² for composites with treated fibers and high density of matrix cracks. Also, it was found that an analysis of the strain energy release rate is more applicable to composites with strong interfaces whereas the J-integral approach is more applicable to composites with weak interfaces. However, the authors noted that the J-integral approach is only applicable when it is possible to identify a crack length as long as the characteristic size of the process zone.

Mackin et al. (Mackin et al., 1995) investigated the notch sensitivity of 2-D CG-NicalonTM/CVI-SiC using X-ray imaging. They found that although this material can redistribute stresses around notches, a stress-concentration still persists and that the damage mechanism responsible for stress-redistribution is less effective than the shear band and multiple matrix cracking mechanisms that occur in other CFCCs.

Goto and Kagawa (Goto and Kagawa, 1996) investigated the notch sensitivity of 2-D CG-NicalonTM/CVI-SiC. Tensile specimens 15 mm wide and 3 mm thick were notched with various notch lengths using a diamond-coated braid. No details were reported about the material and the average size of the notch was 100 μ m and the ratio of notch length to specimen width (a/w) ranged between 0.2 to 0.6. Figure 16 shows the strength results for notched and un-notched specimens along with the line of notch-insensitivity. The results indicate that the material exhibits mild notch sensitivity that decreases with increasing ratio of notch length to specimen width (a/w), but that it never disappears. Goto and Kagawa also developed relationships to estimate the fracture toughness of the material

which agreed well with experimental measurements using single edge-notched specimens. The results are presented in Figure 17 for various values of (a/w) .

Xu et al. (Xu et al., 1999) determined the fracture toughness of carbon fiber-reinforced CVI-SiC matrix composites using a single-edge notched beam in 3-pt bending. The material consisted of a 3-D fiber architecture of T300® carbon fibers coated with a layer of pyrocarbon of unspecified thickness. The specimen dimensions were 2.5 mm x 5 mm x 40 mm, the notch depth to specimen height ratio was 0.5 and the notch was 0.2 mm wide. Fracture toughness values of 11.4 - 16.5 MPa m^{0.5} were obtained.

Shen et al. (Shen et al., 1998) used a J-integral approach to characterize the crack initiation toughness of carbon fiber-reinforced CVI-SiC using compact tension specimens. The material used in this investigation consisted of plain weave fabric (0/90) of T-300 fibers occupying 40% of the composite volume. The thickness of the specimens was 3 mm and the radius of the notch varied between 50 and 900 μm . At each loading point the instantaneous J-integral and crack extension were calculated according to standard test method ASTM E-813 (ASTM, 1990). It was found that the initiation toughness is independent of the notch radius for radii less than 200 μm (20 kJ/m²), and that it increases subsequently for larger notch radii. The dominant energy absorption mechanism was found to be one involving pullout of broken fibers and that the critical notch tip radius is of the same order of magnitude as the average pullout length. These results suggest that the apparent crack blunting is accommodated by the formation and opening of the macroscopic crack and not by the inelastic strain associated with multiple matrix cracking.

Henager and Jones (Henager and Jones, 1993) studied the effect of fiber creep and the oxidation of the fiber coating on the growth of matrix cracks in 2-D CG-Nicalon™/CVI-SiC matrix composites. The material used for their investigation consisted of 8 plies of plain weave fabric with a 1.0 μm -thick carbonaceous fiber coating. Single-edge-notched bend bar specimens were tested in four-point flexure at 1100°C in argon with varying amounts of oxygen. The authors found that crack extension occurs when crack closure forces (fiber bridging) are reduced due to either stress-relaxation in the fibers (because of fiber creep) or removal of the fiber coating by oxidation. Fiber creep was found to control crack growth in argon, while interface removal mechanisms were found to control crack extension in the presence of oxygen.

4.21.2.6 Residual Stresses

Residual stresses and strains exist in composites as a result of the mismatch in thermoelastic properties of the constituents. Upon cooling from the processing temperature, these stresses develop as a consequence of the mutual restraint of the constituents on each other's thermal expansion or contraction.

Steen (Steen and Vallés, 1997) estimated the magnitude of residual stresses in CVI-SiC matrix composites reinforced with Al_2O_3 and graphite fibers, from loading-unloading-reloading mechanical cycles at ambient temperature and 1100°C. The materials studied consisted of plain weave fabric of Sumitomo® fibers occupying 40% of the composite volume or 8-harness satin weave fabric of Bestfight™ graphite fibers filling 44% volume of the composite. Upon unloading at ambient temperature, the curves for the CVI-SiC matrix composite reinforced with alumina fibers were not linear and show an inflection point, i.e., increasing stiffness (see Figure 18) which is not observed at room temperature

for the composite reinforced with graphite fibers. This inflection point, which was believed to result from debris impeding crack closure, is associated with crack closure that result from relief of compressive axial residual stresses in the matrix. This inflection point is not observed at elevated temperature (near the fabrication temperature) because in the absence of residual stresses in the matrix there is no matrix crack closure.

The intersection of the tangent curves to the stress-strain curves provides a good estimate of the magnitude of the residual stress in the matrix. In the case of composites reinforced with alumina fibers, the location of the common intersection indicates that the fibers are under tensile residual stresses and the matrix under compressive residual stresses at ambient temperature, which is the opposite for composites reinforced with carbon fibers. As temperature is increased, the location of the intersection point of the tangents will also change (migrate towards the origin as the fabrication temperature is approached) according to the changes in residual stresses in the fiber and matrix.

4.21.3 PHYSICAL PROPERTIES

4.21.3.1 Transport Properties

Most of the applications for which continuous fiber-reinforced ceramic composites are being considered candidate materials (e.g., heat exchangers, combustor liners in gas turbine engines, filters in a new generation of coal-fueled power plants, containment walls in nuclear fusion reactors) involve elevated temperatures and heat fluxes. As a result of heat fluxes, thermal gradients will develop in these materials, which in turn, will result in the generation of thermal strains and stresses. Among the various material properties and geometric variables that affect the magnitude of these thermal strains and stresses, thermal conductivity is indeed the most important (Hasselman and Donaldson, 1995). In general, high values of thermal conductivity are desired in order to minimize thermal stresses and strains, but the opposite would be true for applications requiring energy conservation.

The method most widely used for the determination of thermal diffusivity of continuous fiber-reinforced CVI-SiC matrix composites is the flash technique. Using this technique, Hasselman and co-workers (Hasselman et al., 1991b; Hasselman et al., 1991c; Hasselman et al., 1991a) determined the thermal diffusivity of 1-D and 2-D (plain weave) CG-Nicalon™ fiber-reinforced CVI-SiC composites using disks 10 mm in diameter and 2.5 mm thick. The density of the samples used for these measurements varied between 2.13 and 2.51 g/cc and measurements on partially-infiltrated specimens demonstrated, as expected, that the thermal diffusivity/conductivity of these materials increases with density. For both 1-D and 2-D materials it was found that the thermal diffusivity parallel to the fiber direction exceeds the corresponding values for heat flow perpendicular to the

fibers (Hasselman et al., 1991b). Furthermore, the thermal conductivity was found to be independent of the nature of the ambient atmosphere for undamaged specimens.

Following heating to temperatures above 1500°C, the thermal conductivity of CG-Nicalon™/CVI-SiC was found to become dependent of the environment. For example, in vacuum it was found to be less than in nitrogen or helium. Furthermore, the thermal diffusivity in the direction transverse to the fibers decreased after the thermal treatment. Scanning electron fractographic analysis revealed that the major microstructural changes resulting from the thermal treatment at 1500°C included debonding of the fibers from the matrix (as a result of fiber densification) as well as matrix cracking. Consistent with micromechanical models, both fiber debonding and matrix cracking were found to contribute to the decrease in the composite thermal diffusivity, because the presence of cracks and interfacial gaps interrupts heat transfer by solid conduction. At the same time, the presence of a gas in these cracks and gaps permits heat conduction across the gap by gaseous conduction, which thereby contributes to the overall composite thermal conductivity. Figures 19 and 20 show the results.

Tawil et al. (Tawil et al., 1985) investigated the transport properties of carbon fiber-reinforced CVI-SiC matrix composites. The material investigated consisted of PAN-precursor carbon fibers arranged in 2-D satin weave fabric occupying 28% of the composite volume. The results for the thermal diffusivity of this material in directions parallel and perpendicular to the fiber directions are shown in Figure 21.

Hasselman et al. (Hasselman et al., 1991a) determined the thermal diffusivity of 2D plain weave fabric of Sumitomo® alumina fiber-reinforced CVI-SiC. Figure 22 shows the

values of the diffusivity of this material as a function of temperature. It was found that heat-treatments above the fabrication temperature resulted in an increase in the thermal diffusivity parallel to the fiber plane and a decrease in the thermal diffusivity transverse to the fiber plane because of fiber recrystallization, matrix cracking and interfacial separation.

Using a Xenon flash lamp Snead and Schwarz (Snead and Schwarz, 1995) determined the thermal conductivity of CVI-SiC matrix composites reinforced with different fibers. The reinforcements investigated included CG-Nicalon™, Hi-Nicalon™ and Amoco K1100 and P55 carbon fibers. The fiber architecture for composites with CG-Nicalon™ and Hi-Nicalon™ fibers consisted of plain weave fabric with each fabric layer rotated 30° with respect to its neighbors. In both cases the fibers were coated with a 0.3 μm-thick layer of carbon and occupied 40% of the composite volume. The fiber architecture of the composite reinforced with graphite fibers consisted of a 3-D unbalanced weave of K1100 and P55 fibers. The P55 fibers were woven in the x and y directions with 2000 fibers/tow, while six tows (1000 fibers/tow) of K1100 were woven through the orthogonal weave in the perpendicular direction (z). The overall fiber volume fraction was 44% of which 7% was in the x and y directions and 86% was in the z-direction. Sample cubes of 1.27 cm on a side were machined for thermal diffusivity measurements for all the materials and the thermal conductivity was determined using a mass average of the specific heats of the fibers and matrix. The thermal conductivity results are listed in Table 12.

Beecher and co-workers (Beecher et al., 1994) investigated the effect of thickness of a carbonaceous fiber coating on the thermal conductivity of CG-Nicalon™ fiber-reinforced

CVI-SiC at ambient temperature using a xenon flash lamp. The material investigated consisted of plain weave fabric of CG-Nicalon™ fibers stacked with each layer rotated 30° with respect to its neighbors. The thicknesses of the fiber coating was varied between 0.03 μm and 1 μm and the resulting range of density and fiber volume fraction in the composites were 2.22-2.65 g/cc 39.5-43.7 %, respectively. It was found that the transverse thermal conductivity, (which was calculated using the estimated composite specific heat obtained from the application of the rule of mixtures) increases with increasing carbon coating thickness from 8.4 W/m K for 0.03 μm to 12.9 W/m K for thickness of 1 μm . The thermal conductivity for a material without fiber coating was found to be 13.4 W/m K. The results are presented in Figure 23.

4.21.3.2 Thermal Expansion

Eckel and Bradt (Eckel and Bradt, 1990) determined the thermal expansion of CVI-SiC matrix composites reinforced with either CG-Nicalon™, Nextel™ 312 or FP alumina fibers between 20°C and 1000°C. Measurements were obtained in air both during heating and cooling using an automatic recording dilatometer at a heating rate of 3°C/min. The fiber architecture of the materials was 4-harness satin weave for the FP fiber-reinforced CVI-SiC and 8-harness satin weave for the other two materials. The specimens were rectangular bars with dimensions of 50 mm x 6 mm x 6 mm, with one of the primary fiber directions parallel to the main direction of the specimens. The average linear coefficient of thermal expansion was determined as a function of temperature five times for the three materials and the results are summarized in Table 13. It was found that for composites with constituents having similar coefficients of thermal expansion, the composite coefficient of thermal expansion predicted from a rule of mixtures agrees well with values measured experimentally. However, for the FP fiber-reinforced CVI-

SiC, where the phases have dissimilar coefficients of thermal expansion, the experimental values didn't agree with the model predictions. Furthermore, the heating/cooling curves exhibited significant hysteresis for this material.

4.21.3.3 Thermal Shock Resistance

Thermal shock resistance is the ability of a solid to withstand sudden changes in temperature either during heating or cooling. Traditionally, thermal shock conditions can be simulated in the laboratory using either water or air after exposure to a furnace environment. However, more extreme conditions, similar to those found in the space shuttle main engines for example, have been obtained using a stationary rocket engine (Eckel et al., 1991). In this case the thermal shock temperature difference was controlled between 1000°C and 2500°C by altering the ratio of oxygen and hydrogen in the 1 second that lasts the test. 2-D NicalonTM/CVI-SiC composites were subjected to these test conditions at temperatures between 1300°C and 2300°C by exposing the leading edge of the gauge section of tensile specimens to the gas stream. It was found that after 50 cycles for $\Delta T = 1700^\circ\text{C}$ there was no change in the tensile strength of the material. However when $\Delta T = 1900^\circ\text{C}$ it resulted in the erosion of the edges of the samples and a reduction of up to 40% of the cross-sectional area and a loss of 35% of their tensile strength. However, the matrix cracking stress decreased with increasing number of cycles.

Kagawa (Kagawa, 1997) investigated the thermal shock behavior of CG-NicalonTM/SiC and found that the critical temperature for the onset of crack growth in 2-D NicalonTM/SiC was lower than that for monolithic SiC. Kagawa observed that damage processes resulting from thermal shock consist of microcracks that initiate from pores in

the matrix, growth of cracks inside and between bundles in the transverse plane, and saturation of microcracks after repeated quenching.

Ellingson and co-workers (Ahuja et al., 1997) determined the thermal diffusivity of 2-D CG-NicalonTM/CVI-SiC after specimens were subjected to thermal shock (in water) for $\Delta T=0, 200, 400, 600, 800$ and 1000°C . Another specimen was water-quenched 4 times at $\Delta T=800^{\circ}\text{C}$. The square specimens consisted of plain weave fabric with each layer rotated 30° with respect to its neighbors and a carbonaceous fiber coating of unspecified thickness. The density of the material was not reported. The thermal diffusivity of as-received material was $5.6 \pm 0.6 \cdot 10^{-6} \text{ m}^2/\text{s}$, and this value was found to remain constant (within scatter) regardless of quench history.

4.21.4 DURABILITY AND RELIABILITY

4.21.4.1 Matrix Cracking

Matrix cracking in CFCCs is very dependent on the microstructure of the composite and the fiber architecture. Guillaumat and Lamon (Guillaumat and Lamon, 1993) identified various stages of the tensile stress-strain curve with the different modes of matrix cracking in 2-D CVI-SiC matrix composites. The material used in their study consisted of plain weave fabric of CG-Nicalon™ fibers coated with a thin layer of pyrocarbon and embedded in a CVI-SiC matrix. The fiber volume fraction was 49%, and the matrix had 16% volume fraction of porosity. The density of the composite was 2.45 g/cc. Samples were polished and etched with Murakami's solution and observations were made using optical microscopy. The porosity in the matrix was characterized and frequency distributions of various types of cracks and other microstructural features were obtained for various stress/strain levels along the stress/strain the tensile curve. Microcracks were observed to initiate first at singularities around macropores at 0.025% deformation, and then propagate across neighboring longitudinal yarns to the nearest macropores. Saturation of macropore-originated microcracks occurred at 0.12% deformation. At larger deformation levels, microcracks formed in the transverse yarns and in the narrow strips of interply matrix located between macropores. The formation of these microcracks stopped at 0.2% deformation. Finally, microcracks appeared randomly in the matrix surrounding the longitudinal bundles for deformations above 0.2% (Guillaumat and Lamon, 1995).

Baste and co-workers (Baste et al., 1993) determined the damage tensor for CVI-SiC matrix composites using ultrasonic methods and correlated it with the various types and orientations of matrix cracks in unidirectional and 2D-CGNicalon™/CVI-SiC. The

authors were able to determine the evolution of the elastic constants as a function of maximum applied stress and the determination of the four parameters required to describe the state of damage of the material.

Mizuno et al. (Mizuno et al., 1996) determined the permanent strains in 2-D CG-Nicalon™/CVI-SiC upon repeated loading/unloading to incrementally larger stresses/strains. Their results are presented in Figure 24 for tests conducted at RT and at 1000°C in argon ($P_{O_2} = 1.2 \times 10^{-1}$ Pa). Although the threshold at 1000°C is higher than at RT, the rate of permanent strain with applied stress is larger than at RT.

Akimune and co-workers (Akimune et al., 1991) investigated the effect of spherical particle impact damage on the tensile strength of CG-Nicalon/CVI-SiC matrix composites. The material studied consisted of eleven layers of plain weave fabric of CG-Nicalon fibers occupying 40% of the volume coated with a thin layer of carbon of unspecified thickness. The tensile strength of the material was found to be unchanged after impact with 1.0 mm diameter partially-stabilized zirconia sphere particles at speeds of 600 m/s. Only a spalling crater and radial cracks were caused by the impact and the impact site was not the origin of the composite failure.

4.21.4.2 Mechanical Cyclic Fatigue

Continuous fiber-reinforced ceramics, like most other structural materials, will be subjected to variable thermal and mechanical loading during their service life. However, the microstructural features and damage mechanisms that are responsible for the tough behavior of continuous fiber-reinforced ceramics (i.e., low interfacial shear stress, long

fiber debond lengths and matrix microcracking) often conflict with the microstructural requirements for optimal fatigue resistance (Holmes and Sorensen, 1995).

In general, fatigue-induced failure of continuous fiber-reinforced ceramics is governed by interface wear and fiber damage rather than matrix crack growth. Moreover, these damage processes are enhanced at elevated temperatures, particularly when the fibers and fiber coating are susceptible to corrosion/oxidation.

Holmes et al. (Shuler et al., 1991) studied the fatigue behavior of carbon fiber-reinforced CVI-SiC and found that at ambient temperature the fatigue limit of this material decreases with increasing frequency. Furthermore, they found that the monotonic tensile strength of specimens increased after enduring 10^6 cycles at a frequency of 10 Hz and a maximum stress of 335 MPa, which is the fatigue limit at low frequency. The material used in their investigations consisted of 26 layers of plain weave fabric (0/90) of T-300 fibers (1000 fibers/tow) occupying 45 % of the composite volume. The stress-strain curves of samples that had been fatigued were almost linear and the increase in monotonic tensile strength after mechanical cyclic fatigue was explained as the result of decreasing stress concentrations near the cross-over points between the 0° and 90° bundles. It is noted that at ambient conditions matrix cracking does not control the life of these materials, but rather other damage modes, such as wear and fiber damage are responsible for composite failure (Reynaud et al., 1993).

Rouby and Reynaud (Reynaud et al., 1994) found that 2D CG-NicalonTM/CVI-SiC composites exhibit a well-defined fatigue limit at room temperature that is larger than the proportional limit stress. For fatigue peak stresses below the fatigue limit, the tangent

moduli at the end of loading and start of reloading was found to decrease gradually with number of cycles but then reached a constant value. For fatigue peak stresses larger than the fatigue limit stress, the stiffness evolved in similar fashion but failure occurred before reaching the stabilization level (Reynaud et al., 1994).

Mizuno and co-workers (Mizuno et al., 1996) studied the mechanical cyclic fatigue behavior of 2-D CG-NicalonTM/CVI-SiC matrix composites at 10 Hz at room temperature and at 20 Hz at 1000°C in argon (at a partial pressure of O₂ of 1.2×10^{-1} Pa) using a sinusoidal waveform and a stress ratio of 0.1. The material used in this study consisted of plain weave fabric coated with a thin layer of carbon. The fiber volume fraction was 40%, the matrix porosity 10% and the density of the composite 2.58 g/cm³. Figure 25 shows a plot of the peak stress versus cycles to failure summarizing the results of this study. Although the ultimate tensile strength and proportional limit stress at 1000°C were higher than those obtained at room temperature, the fatigue limit stress at 1000°C was lower than at room temperature, but this trend was not followed when tests were conducted in ambient air. In reference to Figure 25, note that the fatigue limit stress was higher than the proportional limit stress at room temperature, consistent with the findings of Rouby and co-workers (Reynaud et al., 1994) for 2-D CG-NicalonTM/CVI-SiC matrix composites and Holmes and co-workers (Shuler et al., 1991) for carbon fiber-reinforced CVI-SiC. It was also found that the strength of specimens that survived 10^7 cycles decreased only slightly with respect to the virgin strength of the material.

There has been very limited work dedicated to investigating the simultaneous effect (whether in phase or out of phase) of thermal and mechanical cyclic loading on the properties of fiber-reinforced CVI-SiC composites. In many of the envisioned

applications for fiber-reinforced ceramic matrix composites loading histories involve variable mechanical and thermal loads creating thus the conditions for thermomechanical fatigue. However, the simulation of thermomechanical fatigue loading conditions in laboratory tests is a challenging task. Weinberg et al. (Weinberg et al., 1997) investigated the thermomechanical fatigue of carbon and Nicalon™ fiber-reinforced CVI-SiC to temperatures up to 1455°C. Tests were conducted in both tension and flexure and included the application of variable environmental profiles to simulate re-entry conditions of reusable space vehicles. Eight different material systems were investigated. These included plain weave, filament wound, 5 harness and 8 harness satin weaves, CG-Nicalon™, Hi-Nicalon™, T300® carbon fibers, and carbon and boron nitride fiber coatings. Specimens with 4 to 10 plies and fiber volume fractions between 41 and 48% were evaluated. The failure of carbon-fiber-reinforced CVI-SiC composites occurred mostly during the cooling part of the thermal cycles while Nicalon™ fiber-reinforced CVI-SiC matrix composites failed at elevated temperature, most likely as a result of fiber creep and thermal degradation.

4.21.4.3 Creep and Stress-Rupture.

When fiber-reinforced ceramic matrix composites are subjected to a constant mechanical load at elevated temperature, the compliance of the material typically increases with time. Although this laboratory test is often referred to as “creep” test, and the associated changes in compliance as “creep” strain, the time-dependent deformation of ceramic matrix composites under these conditions arises not only from creep (i.e., flow) of the various constituents, but also from matrix cracking, fiber debonding, fiber sliding and fiber failure. At elevated temperatures, time-dependent matrix cracking (Henager and Jones, 1993) (and therefore compliance changes) can occur at composite stresses lower

than the monotonic proportional limit stress at that particular test temperature as a result of dissimilar creep resistance of the constituents (Lara-Curzio and Ferber, 1994; Holmes and Wu, 1995).

Figure 26 shows the strain histories of 2D CG-Nicalon™ fiber-reinforced CVI-SiC matrix composites at 1204 °C. Note that the curve for the test at 50 MPa exhibits a long transient of continuously decreasing rate of deformation, whereas the curve for the test at 70 MPa exhibits a regime of accelerated deformation prior to failure. Failure 27 shows the corresponding rate of deformation for these two tests.

A standard has been developed within ASTM for the creep and stress-rupture evaluation of fiber-reinforced ceramic matrix composites ASTM C1337 (ASTM, 1997). Provisions have been made for specimen geometry, loading and heating rates, extensometry, etc.

Lamouroux et al. (Lamouroux et al., 1994b) investigated the time-dependent behavior of Sumitomo® fiber-reinforced CVI-SiC under constant load. The fiber architecture of the material consisted of 2D plain weave fabric coated with a carbonaceous layer of thickness of 0.5 to 1 µm. The fiber's volume fraction was 40% and there was 20% porosity in the matrix. Constant stress tests conducted at 1000°C in air showed that the material exhibited continuously increasing compliance with time and that the specimen accumulated as much as 8.5 % deformation after 40 hours at a composite stress of 100 MPa. Prior to failure, a regime of rapid deformation, associated with the progressive rupture of the fibers was observed.

Holmes & Morris (Holmes and Wu, 1995) studied the time-dependent deformation of carbon T-300 fiber-reinforced CVI-SiC at 1400°C in argon with varying amounts of oxygen. The fiber architecture of the material used in the investigation consisted of an angle-interlock 3-D structure with tows containing 3000 fibers in the warp direction and tows with 1000 fibers in the fill direction. The total fiber volume fraction was 45% and the density of the material was 2.05 ± 0.1 g/cc. The deformation of specimens, with the tensile axis parallel to the warp direction, was recorded during tests at 1400°C for constant applied stresses between 45 and 90 MPa. The quasi-steady state rate of deformation at 1400°C when the oxygen concentration was 10 ppm, was found to depend on the applied constant stress as:

$$\frac{d\varepsilon}{dt} = C_1 \sigma^{2.3} \quad (3)$$

while the strength decreased with time as

$$\sigma = C_2 t^{-0.3} \quad (4)$$

It was also found that for a constant applied stress of 50 MPa the failure time increased from 10 hr. when the argon atmosphere contained 10 ppm of O₂, to over 100 hours for argon with 1 ppm of O₂. In air the rupture time at 1400°C and 50 MPa was less than 0.1 h. These results clearly indicate that the term “inert environment” is relative and that these materials, specifically carbon fiber-reinforced CVI-SiC composites are very sensitive to even small concentrations of oxygen at elevated temperatures.

Halbig et al. (Halbig et al., 1997) studied the stress-rupture behavior of carbon fiber-reinforced CVI-SiC in ambient air at temperatures between 350°C to 1500°C and stresses of 69 MPa and 172 MPa. These authors reported that the life of specimens tested at temperatures of 750°C and above was less than 2 hours and that specimens tested at lower temperatures did not failed but lost more than one half of their original strength after a 25 hour-long test. The material used in this investigation consisted of plain weave fabric of T300® carbon fibers, coated with a thin layer of carbon and embedded in a CVI-SiC matrix. Records of the deformation histories of these tests showed that the compliance of the specimens increased continuously with time and that there was accelerated deformation prior to failure consistent with the progressive rupture of the reinforcing fibers.

Recently Lebrun et al. (Lebrun et al., 1999) developed a model to predict the life of carbon fiber-reinforced CVI-SiC composites when subjected to stress-rupture conditions at elevated temperatures. The authors determined that the life of this material is dictated by the oxidation kinetics of the fibers and the fiber coating and by the fraction of fiber breaks. Model predictions were in good agreement with experimental data obtained from the evaluation of minicomposites.

Verrilli et al. (Verrilli et al., 1997) studied the stress-rupture behavior of CG-Nicalon™ fiber-reinforced CVI-SiC in ambient air at temperatures between 500 and 1150°C. Tests were conducted using tensile specimens 152 mm-long with a reduced gauge section consisting of eight plies of 2-D plain weave fabric coated with a 0.1 µm thick layer of carbon. The matrix contained an enhancement for oxidation resistance of proprietary composition³. The results from the stress-rupture tests are summarized in Figure 28 and

indicate a rapid loss of strength with time for stresses larger than 55 MPa. For tests conducted at temperatures above 800°C, the specimens failed outside of the uniformly heated gauge section, which is indicative of the anomalous stress-rupture behavior of these materials at intermediate temperatures.

Experiments conducted by Lara-Curzio and Ferber (Lara-Curzio and Ferber, 1997b) in ambient air revealed that 2-D CG-Nicalon™/CVI-SIC composites exhibited delayed failure even at temperatures as low as 425°C. The material used in that investigation consisted of twelve plies of plain-weave fabric of CG-Nicalon™ fibers coated with a 0.3 μm-thick layer of carbon. The fibers occupied 40% of the volume of the composite and the matrix had 15-20% residual porosity. The resulting strain versus time curves are shown in Figure 29 and reveal well defined stages. In the first stage, the rate of deformation decreases with time, and accelerated deformation is observed just prior to failure. This latter stage is associated with the progressive failure of the reinforcing fibers. Note that although these curves resemble the strain histories that would be obtained from the creep testing of metals, this composite does not undergo creep deformation (in the sense of flow) under these conditions. The changes in compliance with time have been explained in terms of the progressive failure of the fibers as a result of oxidation of the carbonaceous fiber coating and oxidation of the fibers (Lara-Curzio and Ferber, 1997b; Lara-Curzio et al., 1997). This was most evident when analyzing the fracture surface of the specimens which exhibited exaggerated fiber pullout as a result of loss of carbon coating (Figure 30). Examination of the specimens using transmission electron microscopy revealed that in addition to the loss of the carbonaceous fiber coating a silica layer had developed on the surface of the fibers.

Lara-Curzio (Lara-Curzio, 1997) conducted stress rupture tests at 950°C on a material similar to that used by Verrilli et al. (Verrilli et al., 1997). The specimens used were 200 mm-long and had a reduced gauge section. It was found that the compliance of the specimens increased with time and that the rate of deformation accelerated prior to failure. Furthermore, the strength was found to decrease with time as

$$\sigma = C_3 t^{-0.25} \quad (5)$$

The changes in compliance observed experimentally and the time-dependence of strength were explained using a unidirectional model that accounts for the occurrence of matrix cracks, the oxidation (and removal) of a carbonaceous fiber coating followed by a redistribution of internal stresses, the oxidation of the fibers and eventually loss of strength (Lara-Curzio, 1999). Figure 31 shows a schematic of the unit cell used in the model. The combination of Griffith's fracture criterion and the parabolic kinetics associated with the oxidation of SiC-based fibers predicts a rate of loss of strength of the fibers (and composite) that is consistent with the experimental observations. The model predictions are presented in Figure 28 along with experimental results by Lara-Curzio at 950°C (Lara-Curzio, 1997) , Stoloff and co-workers at 1000°C (Lipetzky et al., 1997), Zok and co-workers at 900°C (Steyer et al., 1998) and Heredia et al at 800°C (Heredia et al., 1995).

Pasquier et al. (Pasquier et al., 1998) studied the stress-rupture (static fatigue) of 2-D CG-Nicalon™/CVI-SiC with multilayered fiber coatings of carbon and silicon carbide at temperatures between 700°C and 1200°C and stresses between 60 and 140 MPa. The average fiber volume fraction ranged between 35 and 38% and porosity in the matrix was

less than 10%. The authors classified the observed behavior in 3 different categories depending on the magnitude of stress and temperature. For “Type I” behavior the life of the composites was less than 1 hour and both the elastic modulus and the interfacial shear stress decreased continuously with time until failure. Behavior of Type II and III exhibit two sequential stages: the first stage where both the elastic modulus and the interfacial shear stress decrease with time, and the second stage where both of these quantities increase afterwards. In particular, in type II behavior, the elastic modulus increases in the second stage after reaching a value equal to $0.5v_f E_f$, i.e., when the fibers are completely decouple from the matrix as a result of complete removal of the carbonaceous fiber coating, whereas in type III behavior, the elastic modulus also reaches a minimum value at the end of stage I, but this values is larger than $0.5v_f E_f$. Subsequent increases in elastic modulus and interfacial shear stress result from oxidation of the fibers and the SiC fiber coatings.

Mizuno and co-workers (Zhu et al., 1997; Zhu et al., 1998; Zhu et al., 1999) studied the creep behavior of CG-Nicalon™ fiber-reinforced CVI-SiC. The authors found that for 2-D materials tested in argon at temperatures between 1000°C and 1300°C the minimum rate of deformation and the applied stress were related according to a Monkman-Grant relation, i.e.,

$$t_r \epsilon^{0.72} = C_5 \quad (6)$$

where t_r is the failure time, ϵ the rate of deformation and C_5 a constant. The minimum rate of deformation, the time to failure and the test temperature were also found to be

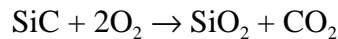
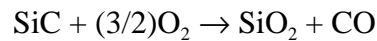
interrelated and could be described using a single Larson-Miller parameter as indicated in Figure 32.

Mizuno and co-workers (Mizuno et al., 1998) also evaluated the stress-rupture behavior of CVI-SiC matrix composites reinforced with Hi-NicalonTM fibers. The material investigated consisted of plain weave fabric coated with 0.2-0.5 μm thick layer of carbon. The fiber volume fraction was 40% and the porosity in the matrix was 9.7%. The specimens were 3.2 mm-thick. Figure 33 shows a plot of stress versus time to rupture from tests conducted in air at 1300°C. Also in the plot are results for regular CG-NicalonTM/CVI-SiC matrix composites and CG-NicalonTM/CVI-SiC matrix composites with the matrix containing an oxidation resistant enhancement of proprietary composition. Although the stress-rupture behavior of Hi-NicalonTM/CVI-SiC and CG-NicalonTM/CVI-SiC with enhancement for oxidation resistance is similar, it is significantly better than the behavior of standard CG-NicalonTM/CVI-SiC matrix material.

4.21.5 ENVIRONMENTAL AND RADIATION EFFECTS ON PHYSICAL AND MECHANICAL PROPERTIES

4.21.5.1 Oxidation and Corrosion

One of the properties that makes SiC attractive for applications in air at elevated temperatures is its excellent resistance to oxidation. The mechanism of passive oxidation of SiC is based on the formation of a protective layer of silica according to the following reactions:



However, despite the remarkable resistance to oxidation (in air) at elevated temperatures and ambient pressure of CVI-SiC, there are certain conditions of stress and temperature for which CVI-SiC matrix composites exhibit severe degradation of mechanical properties as a result of oxidation. These are associated with the ingress of the environment to the interior of the composite and the subsequent oxidation of the fibers and fiber coatings.

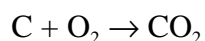
Recently, it has been reported that CVI-SiC and CVI-SiC matrix composites exhibit active oxidation and severe degradation of its integrity and mechanical properties in high-pressure water vapor-containing environments at elevated temperatures [references]. This is significant considering that many of the applications of interest for CVI-SiC matrix composites involve combustion environments (which contain water) and high pressures. The active oxidation of CVI-SiC matrix composites in gas turbine combustion

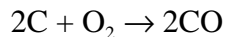
environments (elevated temperatures and high pressures) has been explained using parabolic kinetics. In this case, water vapor reacts with silica to form SiOH_4 which as a gaseous species is removed by the gas stream (Opila, 1997). Similarly, severe corrosion has been found when these materials are exposed to simulated and actual combustion-related environments specially in the presence of alkali (Federer et al., 1985).

Richardson and Kowalik (Richardson and Kowalik, 1997) studied the resistance of CG-Nicalon™ fiber-reinforced CVI-SiC matrix composites containing matrix additions for improved oxidation resistance. They found that Na_2SO_4 does not react with SiC below 900°C . Metallographic observations of specimens subjected to corrosion above 900°C revealed the formation of SiO_2 surface layers including quartz, cristobalite and tridymite and reaction of Na_2SO_4 with the interior phases of the composite.

The degradation of the physical and mechanical properties of continuous fiber-reinforced CVI-SiC composites as a result of oxidation, results from the ingress of the environment to the interior of the composite through matrix cracks, open machined surfaces, and fiber ends. For carbonaceous fiber coatings, oxidation results in the removal of the fiber coating, leaving a gap between the fibers and the matrix that will result in the local redistribution of stresses, because load is transferred between the fibers and the matrix through the fiber coating. Once the fibers are exposed to the environment, the fibers will oxidize (in the case of non-oxide) and lead to loss of fiber strength.

At low temperature carbon consumption is controlled by the kinetics of the reactions





while at high temperatures, oxidation becomes controlled by the diffusion of oxygen through the cracks and the interfacial porosity created by carbon combustion.

Filipuzzi and Naslain (Filipuzzi and Naslain, 1994) developed a thermokinetic chemical analysis to model the oxidation behavior of CVI-SiC matrix composites reinforced with SiC-based fibers and a carbonaceous fiber coating. The analysis, which was conducted for various values of partial pressures of oxygen and temperatures, identified the thickness of the fiber coating that is critical to promote the sealing of channels, created by the removal of the fiber coating, by matrix oxidation. The model predictions were well matched with experimental measurements using a unidirectional material model and Ohmic resistance measurements were correlated with the carbonaceous coating recession distance along the fiber length (Filipuzzi et al., 1994). Self healing behavior was only predicted for temperatures above 1100°C and carbon fiber coatings thicknesses less than 0.1 μm .

Kleykamp and co-workers (Kleykamp et al., 1995) identified the crystallographic phases that formed after CVI-SiC matrix composites are subjected to oxidation. These authors found that the silica layer that forms below 1000°C is amorphous and crystallizes to cristobalite above this temperature. They conducted anisothermal oxidation experiments in air up to 1450°C and the peaks obtained were associated with the oxidation of the free carbon (maximum at 620°C) and the first rapid oxidation of SiC at 1200°C.

The analysis of TGA curves obtained when CG-NicalonTM/CVI-SiC specimens with carbonaceous fiber coatings are subjected to air exposure at elevated temperatures has been correlated with the occurrence of processes at the fiber matrix interface, in particular the oxidation of the fiber coating and formation of SiO₂ in the matrix (Tortorelli et al., 1993). As a result of exposure to air at 950°C it was found that 2-D CG-NicalonTM/CVI-SiC matrix composites with a 0.3µm thick carbonaceous fiber coating specimens lost 40% of their strength after only 15 minutes. These results were correlated with the rapid weight losses recorded during TGA experiments where rapid weight losses are observed during the first hour of the test.

Fox and Nguyen (Fox and Nguyen, 1995) studied the oxidation behavior of CG-NicalonTM/CVI-SiC. The matrix contained “enhancements” of proprietary nature for oxidation purposes³. It was indicated that the enhancement consisted of a boron-based filler that serves as oxygen getter that forms a sealant glass. Tests were conducted at temperatures between 982°C and 1316°C for 100 hours in dry flowing oxygen for periods of up to 100 hrs. At temperatures higher than 1100°C the material was protected and parabolic kinetics were observed. The parabolic rate constant was found to be $7.6 \times 10^{-4} \text{ mg}^2/\text{cm}^4 \text{ h}$ and $1.7 \times 10^{-3} \text{ mg}^2/\text{cm}^4 \text{ h}$ at 1093°C and 1204°C and $3.9 \times 10^{-2} \text{ mg}^2/\text{cm}^4 \text{ h}$ at 1360°C. However, un-reproducible results were obtained at 982°C. Differences were observed depending on the composition of the furnace tube with faster kinetics when using alumina tubes vs. quartz tubes and that the sodium impurities are responsible but don't play a role after 2000 hours at temperatures 1200-1400 °C.

Some of the first studies of environmental effects on the mechanical properties of CVI-SiC matrix composites was conducted by Woodford and co-workers (Woodford et al.,

1992). Tensile strength and elongation were reported for CG-NicalonTM- and carbon fiber-reinforced CVI-SiC composites from room temperature to 1200°C in air. Both composites showed reduced fracture resistance at temperatures above 600°C. The CG-NicalonTM/CVI-SiC composite was resistant to environmental attack during isothermal and cyclic exposures to 1000°C in contrast to composites reinforced with carbon fibers which were severely attacked resulting in fiber oxidation and very low tensile strength. Protective coatings have no significant effect on CG-NicalonTM/CVI-SiC but provide substantial protection for carbon-CVI-SiC. There are indications that the latter system may crack readily as a result of thermal expansion mismatch because even the coated samples degrade on thermal cycling.

Lamoureux and Camus (Lamoureux et al., 1993) studied the oxidation behavior of carbon fiber-reinforced CVI-SiC. They found that diffusion of oxygen to the interior of the composite occurs by diffusion through matrix cracks and that these cracks can form both by the application of stress and from processing as a result of the mismatch in the thermoelastic properties of the constituents. They also found that the reaction of the environment with the fibers results in fiber oxidation and in an effective loss of material.

Lamoureux and Camus (Lamoureux and Camus, 1994) also studied the effect of oxidation on the room temperature tensile properties of the same material after thermal treatments between 700° C and 1400° C. They found that morphological changes in the material were related to the observed changes in the mechanical properties. After treatments at temperatures below 800°C it was found that the fibers that were located near the matrix cracks exhibited notches which translated into drastic loss of tensile strength of the composite. The notching oxidation of the fibers was less extended in air

when compared to exposures in dry oxygen. It was also found that the carbon interface is preferentially consumed near the microcrack tips where free surfaces are present and that locally un-coated fibers get oxidized rapidly in these regions in which the carbon coating has been removed. Exposures to air at temperatures above 1000°C also resulted in a loss of strength but less dramatic than the effect of exposure at intermediate temperatures, although there was evidence of damage of the fibers located at the outer layers of the composite. Degradation of the mechanical properties after exposure at low temperatures was controlled by reaction kinetics between carbon and oxygen whereas during exposure at intermediate temperatures the process was controlled by the diffusion of the gaseous species through the cracked SiC coating. In the latter case degradation was not uniform decreasing gradually from the surface inwards into the specimen. At higher temperatures oxidation of the SiC outer coating and the formation of SiO₂ resulted in the sealing of the interior of the composite (Lamouroux et al., 1994a).

Huger et al. (Huger et al., 1994) studied the oxidation of CG-Nicalon™ fiber-reinforced CVI-SiC with carbonaceous fiber coatings under isothermal conditions using ultrasonic techniques and thermogravimetric analyses. The changes in measured stiffness were correlated with microstructural observations which revealed that the loss of stiffness measured at temperatures above 550°C is associated with the oxidation of the carbonaceous fiber coating, whereas subsequent increases in stiffness at temperatures higher than 750°C were correlated with the growth of silica in the annular pores created around the fibers by the oxidation of the fiber coating.

Bouchetou et al. (Bouchetou et al., 1995) correlated the effect of oxidation on the structural integrity of carbon and Nicalon™ fiber-reinforced CVI-SiC matrix composites

by means of ultrasonic techniques. These authors conducted measurements in air at 815°C at constant stresses above and below the matrix cracking stress. It was found that for all stresses the elastic modulus decreased with time by as much as 30% after 5 hours under a stress of 115 MPa. For a stress of 120 MPa, the specimen failed after just 25 minutes. These tests were accompanied by substantial acoustic emission events. The changes in compliance were explained based on the oxidation of the carbonaceous fiber coating and from the experimental results it was possible to estimate the oxidation rate of the carbon coating. Cyclic thermal measurements between 20°C and 1300°C in argon revealed changes in compliance and hysteretic behavior which were associated with the cracking of the matrix. Chevalier et al. (Chevalier et al., 1998) developed a shear-lag model incorporating the time-dependence of the interfacial parameters to predict the changes in compliance of the composite. In particular, they assume that the interfacial shear stress relaxes with time by as much as 70% after 50 hours when the composite is subjected to a constant stress of 90 MPa. This in turn, predicts a time-dependence of the monotonic tensile stress-strain curves on loading rate.

4.21.5.2 Neutron Irradiation

One of the applications for which fiber-reinforced CVI-SiC composites are currently being considered is for the construction of the plasma-facing first wall, blanket and divertor plate of nuclear fusion reactors. SiC-based materials are attractive for this application because of their potential to retain their strength at elevated temperature and their low neutron activation. However, thermal management requirements require that the material exhibits good thermal conductivity even after prolonged exposure to neutron irradiation.

Snead et al. (Snead et al., 1992b) found that while the stiffness and hardness of CVI-SiC decrease by about 5% after neutron irradiation -to doses of 1 dpa (displacement per atom) at 300°C-, CG-Nicalon™ fibers undergo densification resulting in increases of both Young's modulus (20%) and hardness (40%). At the same time, the strength of the composite was found to decrease by 25% but this reduction in strength was accompanied by a significant increase in fiber pullout length (Snead et al., 1992a). The material investigated had a volume fraction of fibers was 40% which had been coated with a 0.17 μm -thick layer of carbon. The loss of strength was explained based on the loss of stress transfer between the fibers and matrix (because of fiber densification) which is consistent with the long fiber pullout lengths observed. These results were also consistent single-fiber push-out test results which showed that the shear strength had decreased after neutron irradiation (Snead et al., 1992a).

Senor et al. (Senor et al., 1997) measured the thermal expansion of CG-Nicalon™ fiber-reinforced CVI-SiC between ambient temperature and 1000°C after the specimens were irradiated with fast neutrons to 33 dpa at 1000°C. The composites consisted of a triaxial fiber architecture with five times more fibers in the 90° direction than in the 0° direction. The total fiber volume fraction was 40% and the fibers had been coated with a 0.15 μm -thick layer of pyrocarbon. As a result of neutron irradiation there was a complete debonding of the fibers and matrix and the coefficient of thermal expansion of the composite was the same in both directions and essentially identical to that of the matrix.

4.21.6 COMPONENTS AND SPECIAL CONFIGURATIONS

As continuous fiber-reinforced ceramic matrix in general, and CVI-SiC matrix composites in particular, continue to mature, these materials have been used more and more in the fabrication of components for demonstration projects in industrial applications. One example is the fabrication of filters for coal-fired power plants (Judkins et al., 1996). The purpose of these filters is to remove particles from the gas stream before these are fed into a gas turbine. One material that has been considered for this application consists of chopped CG-Nicalon™ fibers fiber embedded in a CVI-SiC matrix. The design requirements for this component involve resistance to cyclic internal pressurization (for cleaning purposes), resistance to thermal shock, resistance to chemical attack in combustion environments, service lives of 20-30 thousand hours. Preliminary characterization work has been focused on the evaluation of these components after exposure in actual service environments for different periods of time. These filters are typically 50 mm diameter, 3 mm wall thickness and lengths in excess of 3 meters. Because of the operating conditions, it is believed that the tensile tangential stress will limit the design of this component. Figure 35 shows a set of tangential stress versus strain curves obtained from the internal pressurization of 25 mm long tubular filter specimens consisting of chopped of CG-Nicalon™ fiber, coated with a thin layer of carbon and embedded in a CVI-SiC matrix. Internal pressurization is achieved by compressing an elastomeric insert (Lara-Curzio unpublished results). The results show the degree of reproducibility achieved in the production of these materials, even in the mode of failure, which occurred at the seam required to form a closed structure. This results highlights important consideration when attempting to use data generated using flat coupons for the prediction of properties of components with complex geometries.

In contrast to this application where the state of stress is relatively simple, in many other applications components will be subjected to multiaxial states of stress which in turn will require the evaluation of special configurations including the evaluation of the component under actual and simulated conditions. Percival et al. (Percival et al., 1997) have developed bi-axial failure maps for 2-D CG-Nicalon™/CVI-SiC matrix composites. These maps have been constructed with tensile, torsion and internal pressurization of tubular specimens. Figure 34 shows one of those failure maps along with a strength criterion.

4.21.7 SUMMARY

Continuous fiber-reinforced CVI-SiC matrix composites exhibit remarkable physical and mechanical properties that are attractive for use in the aerospace and many other industrial applications. Although substantial developments have been achieved over the last 20 years particularly in the area of SiC-based fibers, there is still considerable work needed, particularly in the areas of resistance to aggressive industrial environments, durability and reliability. This work includes the development of oxidation-resistance fiber coatings, oxide fibers with better dimensional and microstructural stability and environmental barrier coatings.

Substantial efforts have also been focused to develop standardized test methods for measurement of physical and mechanical properties. These tests methods will be essential for building data bases once these materials achieve a maturation stage.

TABLES

Direction	Ex (GPa)	Ey (GPa)	Gzx (GPa)	Gxy (GPa)	Gyz (GPa)
x	234.9		78.8	67.9	
y		235.4		68.3	68.3

Table 2.- Elastic properties of CG-Nicalon™/CVI-SiC in ambient air between room temperature and 1200°C (Sakata and Ohnabe, 1997).

	0/90	0/±45/90	±45
Elastic Modulus (GPa)	240.6 (14.5)	219.3 (20)	182.7 (24.1)
Poisson's ratio	0.19 (0.07)	0.19 (0.04)	0.20 (0.02)
Shear Modulus (GPa)	75.8 (25.5)	92.4 (21.4)	101.4 (15.2)

Table 3.- The effect of fiber architecture on the elastic constants of CG-Nicalon™/CVI-SiC matrix composites (Stiff, 1993).

	0/90	0/±45/90	±45
Modulus (GPa)	76	57	56
Tensile Strength (MPa)	425	352	168

Table 4a.- Typical values for Young's modulus, Poisson's ratio and shear modulus along the principal directions of carbon fiber-reinforced CVI-SiC matrix composites.
From DLC. Preliminary Engineering Data for C/SiC

	0/90	0/±45/90	±45
Modulus (GPa)	211	220	210

Table 4b.- Typical values for Young's modulus, Poisson's ratio and shear modulus along the principal directions of carbon fiber-reinforced CVI-SiC matrix composites.
From DLC. Preliminary Engineering Data for C/SiC and CG-Nicalon™/SiC.

	0/90	0/±45/90	±45
Proportional limit stress (MPa)	88.9 (8.9)	80.0 (8.3)	77.9 (4.8)
Tensile Strength (MPa)	248.2 (11.7)	228.2 (10.3)	191.7 (2.1)
Failure Strain (%)	0.44 (0.03)	0.51 (0.08)	0.54 (0.03)

Table 5a.- Effect of fiber architecture on the tensile properties of CG-Nicalon™-reinforced CVI-SiC matrix composites (Stiff, 1993).

	0/90	0/±45/90	±45
Tensile Strength (MPa)	187	167	150

Table 5b. The effect of fiber architecture on the tensile properties of CG-Nicalon™-reinforced CVI-SiC matrix composites (Allied Signal Composites, 1999).

	0/90	0/±45/90	±45
Proportional limit stress (MPa)	39.3 (6.2)	40.7 (9.7)	44.1 (9.0)
Shear Strength (MPa)	95.8 (11.0)	114.5 (11.7)	124.1 (8.3)
Failure Strain (%)	0.62 (0.05)	0.55 (0.03)	0.50 (0.02)

Table 6a.- Effect of fiber architecture on the in-plane shear strength of CG-Nicalon™/CVI-SiC (Stiff, 1993).

	0/90	0/±45/90	±45
Interlaminar Shear Strength (MPa)	38.6 (7.6)	40.7 (5.5)	41.4 (9.0)

Table 6b.- Effect of fiber architecture on the interlaminar shear strength of CG-Nicalon™/CVI-SiC (Stiff, 1993).

Interfacial Shear Stress	Interfacial Debond Energy	Axial Thermal Fiber Residual Stress
42-65 MPa	1.14-1.22 (J/m ²)	-522 - -670 MPa

Table 7.- Interfacial debond energy, interfacial shear stress and fiber residual stress for CG-NicalonTM/CVI-SiC (Sudre et al., 1993)

Microcomposite	Interfacial Shear Stress (MPa)	Debond Energy (J/m ²)
CG-Nicalon TM /C/CVI-SiC	1-21	0-5
CG-Nicalon TM /BN/CVI-SiC	3-24	0-7

Table 8.- Estimates of the interfacial properties of CVI-SiC matrix composites by tensile evaluation of microcomposite specimens (Lamon et al., 1995).

Minicomposite	Estimated Interfacial Shear Stress (MPa)
CG-Nicalon TM /BN/CVI-SiC	25 ± 10
Hi-Nicalon TM / BN/CVI-SiC	15 ± 10
Sylramic®/ BN/CVI-SiC	65 - 175

Table 9.- Interfacial shear stress of BN-coated CG-NicalonTM, Hi-NicalonTM and Sylramic® fiber-reinforced CVI-SiC minicomposites from the analysis of hysteresis loops and measurements of matrix crack spacing (Morscher and Martinez-Fernandez, 1999).

	1-3	1-2
3-D as-received	29.8± 2.5	18.1±0.7
3-D heat treated 1200°C/100 h	13.3± 1.0	10.0±1.2
2-D as-received	16.2±1.7	11.9±0.7
2-D heat treated 1200°C/100 h	8.2±0.5	6.8±1.0

Table 10.- Fracture toughness of CVI-SiC matrix composites with two types of CG-NicalonTM fiber preforms (2-D (0/30/60/90) and 3-D braided preform with a 1x 1 braiding pattern) in two different planes (Yang et al., 1991)

	0/90	0/±45/90	±45
Fracture toughness MPam0.5	27.7 (1.0)	29.9 (1.1)	27.6 (0.6)

Table 11.- Fracture toughness of CG-Nicalon™/CVI-SiC using the conventional LEFM formalism (Stiff, 1993).

	diffusivity (cm ² /s)	conductivity (Wm ⁻¹ K ⁻¹)
Nicalon™/SiC in- plane	0.044	7.4
perpendicular	0.145	25.3
oxidized Nicalon™/SiC in- plane	0.039	6.8
perpendicular	0.141	24.7
k1100/SiC major direction	1.49	214
perpendicular	0.08	12

Table 12.- Thermal conductivity of CVI-SiC matrix composites reinforced with different fibers (Snead and Schwarz, 1995).

	architecture	v _f	density g/cc	α x 10 ⁻⁶ K ⁻¹
FP-SiC	4HSW	.26	2.47	5.30 ± 0.03
Nextel 312-SiC	8HSW	.34	1.98	4.77 ± 0.04
Nicalon™/SiC	8HSW	.31	1.90	4.45 ± 0.07

Table 13.- Coefficient of thermal expansion of CVI-SiC matrix composites reinforced with either CG-Nicalon™, Nextel™ 312 or FP alumina fibers between 20°C and 1000°C (Eckel and Bradt, 1990). The fiber volume fraction and density are also listed.

4.21.8 REFERENCES

Abbe, F. and Chermant, J. L. (1990) *Journal of the American Ceramic Society*, **73**, pp. 2573-2575.

Ahuja, S., Ellingson, W. A., Steckenrider, J. S. and Koch, S. J. (1997) In *Thermal and Mechanical Test methods and Behavior of Continuous Fiber Ceramic Composites*, Vol. ASTM STP 1309 (Eds, Jenkins, M. G., Gonczy, S. T., Lara-Curzio, E., Ashbaugh, N. E. and Zawada, L. P.) American Society for Testing and Materials, .

Akimune, Y., Ogasawara, T., Akiba, T. and Hirosaki, N. (1991) *Journal of Materials Science Letters*, **18**, pp. 682-692.

ASTM (1990) American Society for Testing and Materials, West Conshohocken, PA.

ASTM (1991) American Society for Testing and Materials, West Conshohocken, PA.

ASTM (1995) West Conshohocken, PA.

ASTM (1997) West Conshohocken, PA.

Baste, S., Gerard, A. and Roux, J. (1993) In *Microstructure, Comportements Thermomécaniques et Modélisation des Composites Céramique-Céramique à Fibres*, Vol. 3 (Eds, Chermant, J. L. and Fantozzi, G.) Hermès, Paris, pp. 129-144.

Beecher, S. C., Dinwiddie, R. B. and Lowden, R. A. (1994) In *Thermal Conductivity*, Vol. 22 (Ed, Tong, T. T.) Technomic, Tempe, Arizona, pp. 324-334.

Bouchetou, M. L., Cutard, T., Huger, M., Fargeot, D. and Gault, C. (1995) *Ceramic Transactions*, **57**, pp. 181-190.

Camus, G. and Barbier, J. E. (1995) *Ceramic Transactions*, **57**, pp. 407-412.

Camus, G., Guillaumat, L. and Baste, S. (1996) *Composites Science and Technology*, **59**, pp. 1363-1372.

Carpenter, H. W. and Buhlen, J. W. (1992) *Ceramic Engineering and Science Proceedings*, **13**, pp. 238-256.

Carpenter, H. W., Buhlen, J. W. and Steffier, W. S. (1993) U.S.

Chevalier, J., Huger, M., Fargeot, D. and Gault, C. (1998) *Journal of the European Ceramic Society*, **18**, pp. 1857-1867.

Chulya, A., Gyekenyesi, J. Z. and Gyekenyesi, J. P. (1992) *Ceramic Engineering and Science Proceedings*, **13**, pp. 420-432.

Droillard, C. (1993) University of Bordeaux, .

Droillard, C. and Lamon, J. (1996) *Journal of the American Ceramic Society*, **79**, pp. 849-858.

- Droillard, C., Voisard, P., Heibst, C. and Lamon, J. (1995) *Journal of the American Ceramic Society*, **78**, pp. 1201-1211.
- Eckel, A. J. and Bradt, R. C. (1990) *Journal of the American Ceramic Society*, **73**, pp. 1334-1338.
- Eckel, A. J., Herbell, T. P. and Generazio, E. R. (1991) *Ceramic Engineering and Science Proceedings*, **12**, pp. 1500-1508.
- Effinger, M. R., Tucker, D. S. and Barnett, T. R. (1996) *Ceramic Engineering and Science Proceedings*, **17**, pp. 316-323.
- El Bouazzaoui, R., Baste, S. and Camus, G. (1996) *Composites Science and Technology*, **56**, pp. 1373-1382.
- Evans, A. G., Zok, F. W. and Mackin, T. J. (1995) In *High Temperature Mechanical Behavior of Ceramic Composites*(Eds, Nair, S. V. and Jakus, K.) Butterworth-Heinemann, Newton, MA, pp. 3-86.
- Fang, N. J. J. and Chou, T. W. (1993) *Journal of the American Ceramic Society*, **76**, pp. 2539-2548.
- Federer, J. I., Robbins, J. M., Jones, P. J. and Hamby, C. (1985) Oak Ridge National Laboratory, Oak Ridge.
- Filipuzzi, L., Camus, G., Naslain, R. and Thebault, J. (1994) *Journal of the American Ceramic Society*, **77**, pp. 459-466.
- Filipuzzi, L. and Naslain, R. (1994) *Journal of the American Ceramic Society*, **77**, pp. 467-480.
- Fitzer, E. (1988) In *Whisker- and Fiber-Toughened Ceramics*(Eds, Bradley, R. A., Clark, D. E., Larsen, D. C. and Stiegler, J. O.) ASM International, Oak Ridge, TN, pp. 165-192.
- Fox, D. and Nguyen, Q. N. (1995) *Ceramic Engineering and Science Proceedings*, **16**, pp. 877-884.
- Gomina, M., Themines, D., Chermant, J. L. and Osterstock, F. (1987) *International Journal of Fracture*, **34**, pp. 219-228.
- Goto, K. and Kagawa, Y. (1996) *Materials Science and Engineering A*, **211**, pp. 72-81.
- Guillaumat, L. and Lamon, J. (1993) In *Microstructure, Comportements Thermomécaniques et Modélisation des Composites Céramique-Céramique à Fibres*, Vol. 3 (Eds, Chermant, J. L. and Fantozzi, G.) Hermès, Paris, pp. 159-172.
- Guillaumat, L. and Lamon, J. (1995) *Ceramic Transactions*, **57**, pp. 215-220.
- Halbig, M. C., Brewer, D. N., Eckel, A. J. and Cawley, J. D. (1997) *Ceramic Engineering and Science Proceedings*, **18**, pp. 547-554.

- Hasselman, D. P. H. and Donaldson, K. Y. (1995) In *Handbook on Continuous Fiber-Reinforced Ceramic Matrix Composites*(Eds, Lehman, R. L., El-Rahaiby, S. K. and Wachtman, J. B.) The American Ceramic Society, Westerville, OH, pp. 547-583.
- Hasselman, D. P. H., Venkateswaran, A. and Tawil, H. (1991a) *Journal of the American Ceramic Society*, **74**, pp. 1631-1634.
- Hasselman, D. P. H., Venkateswaran, A., Yu, M. H. and Tawil, H. (1991b) *Ceramic Engineering and Science Proceedings*, **12**, pp. 2251-2261.
- Hasselman, D. P. H., Venkateswaran, A., Yu, M. H. and Tawil, H. (1991c) *Journal of Materials Science Letters*, **10**, pp. 1037-1042.
- Hay, R. S. (1995) *Acta Materialia*, **43**, pp. 3333-3347.
- Henager, C. H. and Jones, R. H. (1993) *Ceramic Engineering and Science Proceedings*, **14**, pp. 408-415.
- Heraud, L. and Spriet, P. (1988) In *Whisker- and Fiber-Toughened Ceramics*(Eds, Bradley, R. A., Clark, D. E., Larsen, D. C. and Stiegler, J. O.) ASM International, Oak Ridge, TN, pp. 217-224.
- Heredia, F. E., McNulty, J. C., Zok, F. W. and Evans, A. G. (1995) *Journal of the American Ceramic Society*, **78**, pp. 2097-2100.
- Holmes, J. W. and Sorensen, B. F. (1995) In *High Temperature Mechanical Behavior of Ceramic Composites*(Eds, Nair, S. V. and Jakus, K.) Butterworth-Heinemann, Newton, MA, pp. 261-326.
- Holmes, J. W. and Wu, X. (1995) In *High Temperature Mechanical Behavior of Ceramic Composites*(Eds, Nair, S. V. and Jakus, K.) Butterworth-Heinemann, Newton, MA, pp. 261-326.
- Hsu, D. K., Miriyala, N., Snead, L. L. and Lowden, R. A. (1995) *Journal of Nuclear Materials*, **219**, pp. 93-100.
- Huger, M., Fargeot, D. and Gault, C. (1994) *Journal of the American Ceramic Society*, **77**, pp. 2554-2560.
- Jacques, S., Guette, A., Langlais, F. and Naslain, R. (1997) *Key Engineering Materials*, **127**, pp. 543-550.
- Judkins, R. R., Stinton, D. P., Smith, R. G., Fischer, E. M. and Eaton, J. H. (1996) *Journal of Engineering for Gas Turbines and Power*, **118**, pp. 495-499.
- Kagawa, Y. (1997) *Composites Science and Technology*, **57**, pp. 607-611.
- Kleykamp, H., Schauer, V. and Skokan, A. (1995) *Journal of Nuclear Materials*, **227**, pp. 130-137.

- Lackey, W. J. and Starr, T. L. (1990) In *Fiber Reinforced Ceramic Composites. Materials Processing and Technology*(Ed, Mazdiyasni, K. S.) Noyes Publications, Park Ridge, NJ, pp. 397-450.
- Lacombe, A. and Bonnet, C. (1990) In *AIAA Second International Aerospace Planes Conference* Orlando, FL.
- Lacombe, A. and Rouges, J. M. (1990) In *Space programs and Technologies Conference '90* Huntsville, Al.
- Lamon, J., Rebillat, F. and Evans, A. G. (1995) *Journal of the American Ceramic Society*, **78**, pp. 401-405.
- Lamoureux, F., Bertrand, S., Pailler, R., Naslain, R. and Cataldi, M. (1999) *Composites Science and Technology*, **59**, pp. 1073-1085.
- Lamoureux, F., Bourrat, X., Naslain, R. and Sevely, J. (1993) *Carbon*, **31**, pp. 1273-1288.
- Lamoureux, F. and Camus, G. (1994) *Journal of the European Ceramic Society*, **14**, pp. 177-188.
- Lamoureux, F., Camus, G. and Thebault, J. (1994a) *Journal of the American Ceramic Society*, **77**, pp. 2049-2057.
- Lamoureux, F., Steen, M. and Vallés, J. L. (1994b) *Journal of the European Ceramic Society*, **14**, pp. 529-537.
- Lara-Curzio, E. (1997) *Journal of the American Ceramic Society*, **80**, pp. 3268-3272.
- Lara-Curzio, E. (1999) *Composites Part A*, **30**, pp. 549-554.
- Lara-Curzio, E. and Ferber, M. K. (1994) *Ceramic Engineering and Science Proceedings*, **15**, pp. 65-75.
- Lara-Curzio, E. and Ferber, M. K. (1995) In *Numerical Analysis and Modeling of Composite Materials*(Ed, Bull, J. W.) Blackie Academic & Professional, London, pp. 357-399.
- Lara-Curzio, E. and Ferber, M. K. (1997a) In *Thermal and Mechanical Test Methods and Behavior of Continuous Fiber Ceramic Composites*, Vol. ASTM STP 1309 (Eds, Jenkins, M. G., Gonczy, S. T., Lara-Curzio, E., Ashbaugh, N. E. and Zawada, L. P.) American Society for Testing and Materials, West Conshohocken, PA.
- Lara-Curzio, E. and Ferber, M. K. (1997b) *Journal of Materials Science Letters*, **16**, pp. 23-26.
- Lara-Curzio, E., Ferber, M. K., Besmann, T. M., Rebillat, F. and Lamon, J. (1995) *Ceramic Engineering and Science Proceedings*, **16**, pp. 597-612.

- Lara-Curzio, E., Ferber, M. K. and Lowden, R. A. (1994) *Ceramic Engineering and Science Proceedings*, **15**, pp. 989-1000.
- Lara-Curzio, E., Ferber, M. K. and Tortorelli, P. F. (1997) *Key Engineering Materials*, **127-131**, pp. 1069-1082.
- Lara-Curzio, E. and Jenkins, M. G. (1999) *Composites Part A*, **30**, pp. 561-567.
- Lebrun, G. A., Lamouroux, F. and Lamon, J. (1999) In *Annual meeting of the American Ceramic Society* Indianapolis, IN.
- Lee, K. N., Jacobson, N. S. and Miller, R. A. (1994) *MRS Bulletin*, **October 1994**, pp. 35-38.
- Lee, W. Y., Lara-Curzio, E. and More, K. L. (1998) *Journal of the American Ceramic Society*, **81**, pp. 717-720.
- Lipetzky, P., Stoloff, N. S. and Dvorak, G. J. (1997) *Ceramic Engineering and Science Proceedings*, **18**, pp. 355-362.
- Lowden, R. A., Schwarz, O. J. and More, K. L. (1993) *Ceramic Engineering and Science Proceedings*, **14**, pp. 375-384.
- Lowden, R. A., Stinton, D. P. and Besmann, T. M. (1995) In *Handbook on Continuous Fiber-Reinforced Ceramic Matrix Composites* (Eds, Lehman, R. L., El-Rahaiby, S. K. and Wachtman, J. B.) The American Ceramic Society, Westerville, OH, pp. 205-268.
- Mackin, T. J., Purcell, T. E., He, M. Y. and Evans, A. G. (1995) *Journal of the American Ceramic Society*, **78**, pp. 1719-1728.
- Mizuno, M., Nagano, Y., Usami, H. and Kagawa, Y. (1994) *Ceramic Engineering and Science Proceedings*, **15**, pp. 859-866.
- Mizuno, M., Zhu, S., Kagawa, Y. and Kaya, H. (1998) *Journal of the European Ceramic Society*, **18**, pp. 1869-1878.
- Mizuno, M., Zhu, S., Nagano, Y., Sakaida, Y. and Watanabe, M. (1996) *Journal of the American Ceramic Society*, **79**, pp. 3065-3077.
- Moore, A. W., Sayir, H., Farmer, S. C. and Morscher, G. N. (1995) *Ceramic Engineering and Science Proceedings*, **16**, pp. 409-416.
- Morscher, G. N. and Martinez-Fernandez, J. (1999) *Journal of the American Ceramic Society*, **82**, pp. 145-155.
- Nair, S. V. and Wang, Y. L. (1992) *Ceramic Engineering and Science Proceedings*, **13**, pp. 433-441.
- Nair, S. V. and Wang, Y. L. (1998) *Journal of the American Ceramic Society*, **81**, pp. 1149-1156.

- Naslain, R. (1995) *Ceramic Transactions*, **58**, pp. 23-29.
- Naslain, R., Dugne, O., Guette, A., Sevely, J., Brosse, C. R., et al. (1991) *Journal of the American Ceramic Society*, **74**, pp. 2482-2488.
- Ogbuji, L. U. J. T. (1995) *Ceramic Engineering and Science Proceedings*, **14**, pp. 497-505.
- Opila, E. J. (1997) *Journal of the American Ceramic Society*, **80**, pp. 197-205.
- Pasquier, S., Lamon, J. and Naslain, R. (1998) *Composites Part A*, **29A**, pp. 1157-1164.
- Percival, M. J. L., Claxton, E., Gabelotaud, S., Dambrine, B. and Maire, J. F. (1997) *Key Engineering Materials*, **127-131**, pp. 791- 798.
- Piccola, J. P., Jenkins, M. G. and Lara-Curzio, E. (1997) In *Thermal and Mechanical Test Methods and Behavior of Continuous Fiber Ceramic Composites*, Vol. STP 1309 (Eds, Jenkins, M. G., Gonczy, S. T., Lara-Curzio, E., Ashbaugh, N. E. and Zawada, L. P.) ASTM, .
- Raghuraman, S., Lara-Curzio, E. and Ferber, M. K. (1996) *Ceramic Engineering and Science Proceedings*, **17**, pp. 147-156.
- Rebillat, F., Lamon, J., Naslain, R., Lara-Curzio, E., Ferber, M. K., et al. (1998a) *Journal of the American Ceramic Society*, **81**, pp. 965-978.
- Rebillat, F., Lamon, J., Naslain, R., Lara-Curzio, E., Ferber, M. K., et al. (1998b) *Journal of the American Ceramic Society*, **81**, pp. 965-978.
- Reynaud, P., Rouby, D. and Fantozzi, G. (1993) In *Microstructure, Comportements Thermomécaniques et Modélisation des Composites Céramique-Céramique à Fibres*, Vol. 3 (Eds, Chermant, J. L. and Fantozzi, G.) Hermès, Paris, pp. 191-206.
- Reynaud, P., Rouby, D. and Fantozzi, G. (1994) *Scripta Materialia*, **31**, pp. 1061-1066.
- Rice, R. W. (1987) The United States of America as represented by the Secretary of the Navy (Washington, DC), U.S.
- Richardson, G. and Kowalik, R. W. (1997) *Ceramic Engineering and Science Proceedings*, **18**, pp. 599-606.
- Sakata, M. and Ohnabe, H. (1997) In *Thermal and Mechanical Test Methods and Behavior of Continuous Fiber Ceramic Composites*, Vol. STP 1309 (Eds, Jenkins, M. G., Gonczy, S. T., Lara-Curzio, E., Ashbaugh, N. E. and Zawada, L. P.) ASTM, .
- Sawyer, J. W. (1988) NASA, Hapton, VA.
- Senor, D. J., Trimble, D. J. and Newsome, G. A. (1997) *Ceramic Engineering and Science Proceedings*, **18**, pp. 591-598.

- Shen, J. Y., Hirth, J. P., Zok, F. W. and Heathcote, J. A. (1998) *Scripta Materialia*, **38**, pp. 15-19.
- Shuler, S. F., Holmes, J. W. and Wu, X. (1991) *Journal of the American Ceramic Society*, , pp. .
- Snead, L. L. and Schwarz, O. J. (1995) *Journal of Nuclear Materials*, **219**, pp. 3-14.
- Snead, L. L., Steiner, D. and Zinkle, S. J. (1992a) *Journal of Nuclear Materials*, **191-194**, pp. 566-570.
- Snead, L. L., Zinkle, S. J. and Steiner, D. (1992b) *Journal of Nuclear Materials*, **191-194**, pp. 560-565.
- Steen, M. and Vallés, J. L. (1997) In *Thermal and Mechanical Test Methods and Behavior of Continuous Fiber Ceramic Composites*, Vol. STP 1309 (Eds, Jenkins, M. G., Gonczy, S. T., Lara-Curzio, E., Ashbaugh, N. E. and Zawada, L. P.) American Society for Testing and Materials, .
- Steif, P. S. and Trojnacki, A. (1994) *Journal of the American Ceramic Society*, **77**, pp. 221-229.
- Steyer, T. E., Zok, F. W. and Walls, D. P. (1998) *Journal of the American Ceramic Society*, **81**, pp. 2140-2146.
- Stiff, W. S. (1993) *Ceramic Engineering and Science Proceedings*, **14**, pp. 1045-1057.
- Stull, K. R. and Parvizi-Majidi, A. (1991) *Ceramic Engineering and Science Proceedings*, **12**, pp. 1452-1461.
- Sudre, O., Parlier, M. and Bouillon, E. (1995) *Ceramic Transactions*, **57**, pp. 389-394.
- Sudre, O., Passilly, B. and Parlier, M. (1993) *Ceramic Engineering and Science Proceedings*, **14**, pp. 180-187.
- Tawil, H., Bentsen, L. D., Baskaran, S. and Hasselman, D. P. H. (1985) *Journal of Materials Science*, **28**, pp. 3201-3212.
- Tortorelli, P. F., Nijhawan, S., Riester, L. and Lowden, R. A. (1993) *Ceramic Engineering and Science Proceedings*, **14**, pp. 358-366.
- Verrilli, M. J., Calomino, A. M. and Brewer, D. N. (1997) In *Thermal and Mechanical Test Methods and Behavior of Continuous Fiber Ceramic Composites*, Vol. ASTM STP 1309 (Eds, Jenkins, M. G., Gonczy, S. T., Lara-Curzio, E., Ashbaugh, N. E. and Zawada, L. P.) American Society for Testing and Materials,, .
- Weddell, J. K. and Ahluwalia, K. S. (1994) In *Moving Forward With 50 Years of Leadership in Advanced Materials*, Vol. 39-II Society for the Advancement of Material and Process Engineering, P.O. Box 2459, Covina, California 91722, USA, Anaheim, California, USA.

- Weinberg, D. J., Myers, F. K. and Holmes, J. W. (1997) *Ceramic Engineering and Science Proceedings*, **18**, pp. 555-569.
- Woodford, D. A., Van Steele, D. R., Brehm, J. and Palko, J. (1992) *Ceramic Engineering and Science Proceedings*, **13**, pp. 752-759.
- Xu, Y., Cheng, L., Zhang, L. and Yan, D. (1999) *Key Engineering Materials*, **164-165**, pp. 73-76.
- Yang, J. M., Ling, W., Shih, C. J., Kai, W., Jeng, S. M., et al. (1991) *Journal of Materials Science*, **26**, pp. 2954-2960.
- Zhu, S., Mizuno, M., Kagawa, Y. and Mutoh, Y. (1999) *Composites Science and Technology*, **59**, pp. 833-851.
- Zhu, S., Mizuno, M., Nagano, Y., CAO, J., Kagawa, Y., et al. (1998) *Journal of the American Ceramic Society*, **81**, pp. 2269-2277.
- Zhu, S., Mizuno, M., Nagano, Y., Kagawa, Y. and Kaya, H. (1997) *Composites Science and Technology*, **57**, pp. 1629-1637.